

Fault-zone structures and solution-mass-transfer cleavage in Late Cretaceous nappes, San Juan Islands, Washington

Mark T. Brandon¹, Darrel S. Cowan², and Jeffrey G. Feehan¹

¹ Department of Geology and Geophysics, Yale University, P.O. Box 208109, New Haven, CT 06520-8109

² Department of Geological Sciences, University of Washington, AJ-20, Seattle, WA 98195

Introduction

This text supports a two-day field trip to examine mesoscopic structures developed during Late Cretaceous thrust faulting and regional shortening. These structures are relevant to two topics. First, asymmetric folds and Riedel composite structures in brittle shear zones, and a more widely developed solution-mass-transfer (SMT) cleavage, collectively provide kinematic evidence for the direction and sense of slip along thrust faults and for the orientation of regional shortening in a major zone of collision in the Northwest Cordillera. Second, strain analysis of the cleavage provides insights into the role of fluid-driven mass transfer in a growing accretionary wedge.

The first part of the article summarizes the regional setting of the field trip localities, introduces the controversy regarding transport directions, and reviews the timing of deformational and metamorphic events. The next part introduces the background and techniques used for kinematic analysis of mesoscale fault-zone structures, and for strain analysis of the SMT cleavage. The concluding field guide describes field trip stops and includes directions that allow

self-guided access by car or bicycle. Note that the introduction is after Cowan and Brandon (1994) with the kind permission of *American Journal of Science*.

Geologic Overview of the Cascade Orogen

The San Juan Islands are part of the Cascade orogen, which lies at the southern end of a 1200 km-long intra-Cretaceous orogenic belt extending from northwestern Washington and southwestern British Columbia to southeastern Alaska (Rubin and others, 1990). At about latitude 49°N, the orogen can be divided into four generally northwest-striking tectonic zones (Fig. 1 shows the western two of these zones). The westernmost zone consists of lower Paleozoic to Middle Jurassic rocks of Wrangellia, which is part of the larger Insular superterrane. Wrangellia is unconformably overlain by the Nanaimo Group, a synorogenic basal sequence that formed adjacent to and received detritus from the San Juan-Cascade nappes. Inboard of Wrangellia is the San Juan-Cascade thrust system, comprising Late Cretaceous thrust faults and nappes of the San Juan Islands and Northwest Cascade Mountains; this

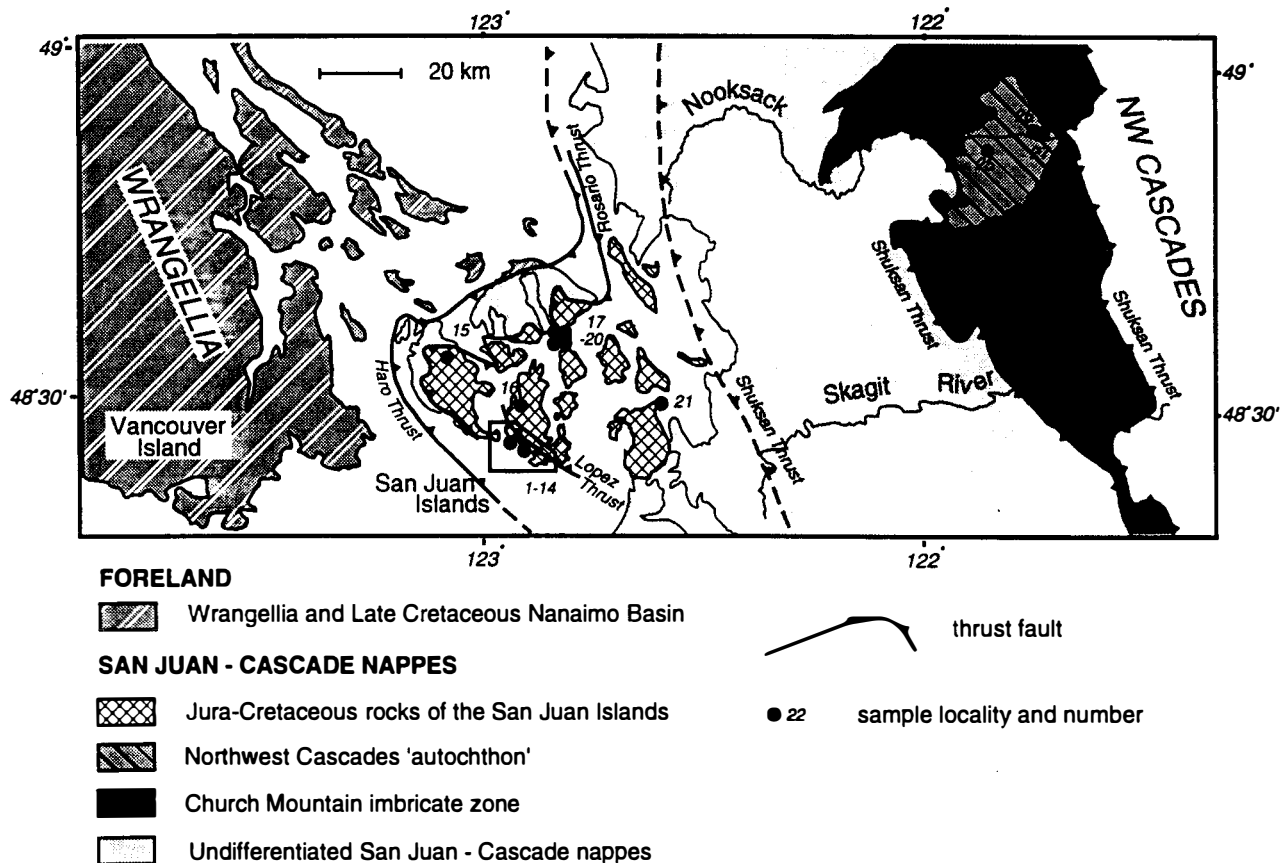


Figure 1. Generalized geologic map of the San Juan Islands and Northwest Cascade Mountains. Dots and numbers indicate samples for strain study (see Table 1). After Misch (1966), Brown and others (1987), Brandon and others (1988), and McGroder (1991).

system developed mainly during the interval 100 to 84 Ma (e.g., Misch, 1966; Brandon and others, 1988; Brandon, 1989). The nappes within this zone were derived from a diverse assemblage of older terranes ranging in age from early Paleozoic to latest Early Cretaceous. The system as a whole appears to structurally overlie the more outboard Wrangellia terrane (Palumbo and Brandon, 1990). The next zone to the northeast, the Cascade metamorphic core, was affected by high-temperature metamorphism, crustal thickening, and plutonism during the Late Cretaceous and early Tertiary (e.g., Misch, 1966; Babcock and Misch, 1988; Haugerud and others, 1991; Miller and others, 1993). The easternmost zone is the eastern Cascade fold belt (McGroder, 1989), consisting of a faulted and folded sequence of Triassic to Upper Cretaceous (Cenomanian) sedimentary and volcanic rocks. Deformation there occurred mainly between 100 and 88 Ma.

The relationship among these elements, and particularly between the San Juan-Cascade thrust system and the metamorphic core, is currently controversial. Although all workers agree that Cretaceous faulting played an important role in fashioning the structure of this belt, there has been considerable disagreement about the orogenic displacements within it. The *contraction model* (Fig. 2A), advocated originally by Misch (1966) and subsequently by Brandon and Cowan (1985), Brandon and others (1988), Brandon (1989), McGroder (1991), and Journeay and Friedman (1993), postulates that the entire orogen formed by large-scale, southwest-northeast contraction which drove the San Juan-Cascade nappes over (Brandon and Cowan) or out of (McGroder; Journeay) the metamorphic core and onto the adjacent Wrangellia terrane. The implied transport direction of the nappes would have been dominantly

top-to-the-southwest. Orogenic contraction is attributed to the collision of Wrangellia against North America (e.g., Davis and others, 1978; Monger and others, 1982). The contraction model accounts for the large amount of orogenic shortening recorded by the San Juan-Cascade thrust system, probably on the order of 200 to 400 km (e.g., Brandon, 1989; McGroder, 1991).

An alternative model (Fig. 2B), advocated by Brown (1987), Smith (1988), Brown and Talbot (1989), and Maekawa and Brown (1991), proposes that the San Juan-Cascade nappes developed in a generally northwest-striking transcurrent shear zone, and that the nappes were driven to the northwest onto a Wrangellia terrane that had already been accreted to North America. This model, which we refer to as the *transcurrent model*, implies a transform boundary to the east, separating the northwest-moving nappes from a fixed North America. This boundary might correspond to the Cascade metamorphic core, which Brown and Talbot (1989) interpreted as a broad, right-lateral shear zone.

A critical difference between the contraction and transcurrent models is the predicted direction of fault slip within the San Juan-Cascade system. The contraction model requires that slip between the nappes was dominantly top-to-the-southwest. The transcurrent model emphasizes dextral slip on high-angle faults and shear zones throughout the Cascade orogen. Proponents of the transcurrent model have conceded that there are thrust faults present in the San Juan-Cascade system, but they consider these to be local features associated with left-stepping jogs within a wide system of dextral transcurrent faults (Maekawa and Brown, 1991). In the transcurrent model, displacements on thrust faults should be top-to-the-northwest. Our kinematic analysis

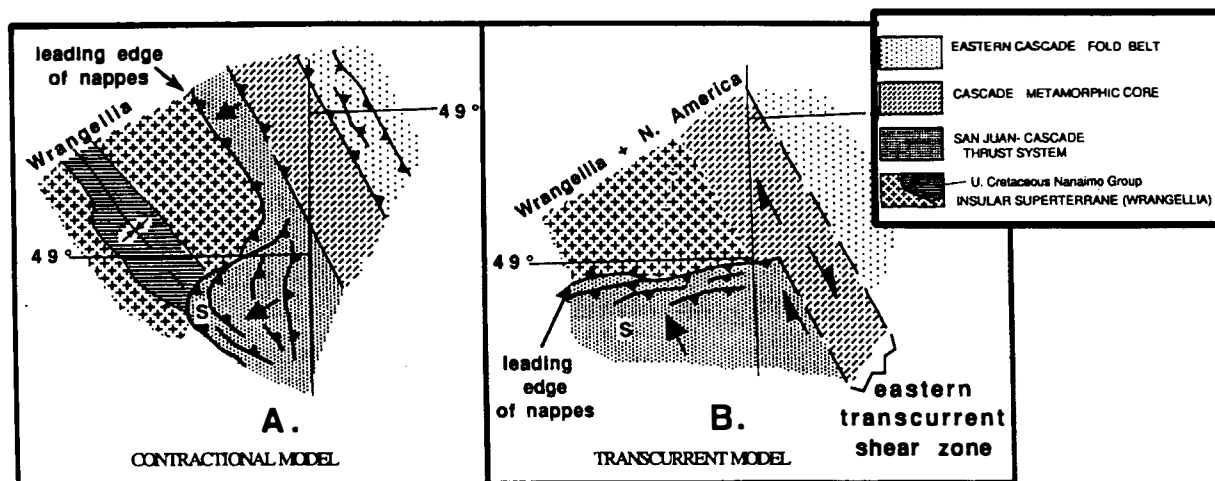


Figure 2. Schematic maps depicting contrasting interpretations of the Late Cretaceous Cascade orogen. Large arrows indicate directions of relative transport. Note that Cenozoic motion on the Fraser-Straight Creek fault has been restored, as indicated by the offset in the 49°N parallel. The San Juan Islands are marked with an "S". (A) In the *contractional model* (Brandon and Cowan, 1985; McGroder, 1991), the Cascade orogen formed by northeast-southwest contraction associated with collision of Wrangellia and top-to-the-southwest transport of the San Juan-Cascade nappes. The Nanaimo Group would represent a foreland basin that formed in front of the advancing nappes. (B) In the *transcurrent model* (Brown, 1987; Brown and Talbot, 1989; Maekawa and Brown, 1991), the Cascade orogen marks the trace of a major northwest-southeast transcurrent shear zone. In particular, the Cascade metamorphic core is envisaged to be a broad ductile shear zone (Brown and Talbot, 1989) which separated a north-moving assemblage of allochthonous terranes from a relatively fixed continental interior to the east. Thrust faults in the San Juan Islands have been interpreted by Maekawa and Brown (1991) to be a system of "step-over" faults which transferred dextral slip from the Cascade core to the west side of Wrangellia. If correct, the San Juan thrusts would have a slip direction of top-to-the-northwest.

of mesoscale fault-zone structures, which we will observe at two field stops, addresses the controversial issue of slip direction.

Nappes and Thrust Faults in the San Juan Islands

Over the last 15 years, the geology of the San Juan Islands has been scrutinized by several research groups. Detailed field mapping and extensive paleontological and isotopic dating have yielded a fairly complete understanding of the general geology of the area. Available information was compiled and synthesized by Brandon and others (1988) and Brandon (1989); these sources provide the primary basis for the following summary.

The geology is characterized by a stacked sequence of thrust nappes (Fig. 3). Each nappe is dominated by a stratigraphically related group of rock units. At present, the nappes are shaped into broad folds that trend and plunge gently to the southeast, and have wavelengths of about 12 km. These folds are inferred to be early Tertiary in age because they are similar both in style and orientation to folds in the Upper Cretaceous Nanaimo Group and the Eocene Chuckanut Group exposed on the mainland east of the San Juan Islands (England and Calon, 1991).

Because the faults at the boundaries of the thrust nappes juxtapose unrelated tectonostratigraphic units, we conclude that they have accommodated large amounts of slip, probably in excess of tens of kilometers (see below for specific estimates). Within the nappes, there is evidence for local imbrication and faulting, but the slip on these internal structures must be relatively minor because stratigraphic offsets are small or not apparent. On this basis, we distinguish between large-slip faults, which commonly form the major terrane-bounding structures, and small-slip faults, which offset or imbricate a given rock unit but do not juxtapose unrelated terranes.

Four large-slip faults have been recognized in the San Juan Islands: the Haro, Orcas, Rosario, and Lopez thrusts (Fig. 3). Of these, the Rosario and Lopez thrusts are exceptionally well exposed in wavecut outcrops along the southwestern coasts of San Juan and Lopez island; both faults will be visited on the field trip.

Rosario Fault Zone

The Rosario fault zone (Fig. 3) has a sinuous trace that extends about 65 km across the San Juan Islands. The hangingwall consists of the upper Mesozoic Constitution Formation, an interbedded sequence of volcaniclastic sandstone, mudstone, and minor ribbon chert and pillow basalt. The footwall is composed of the Lower Permian to

Middle Jurassic Deadman Bay terrane, composed mainly of ribbon chert with subordinate pillow basalt and limestone. In our mapping, we have identified a specific fault surface, the Rosario thrust (Figs. 3 and 13), which corresponds to the upper limit of Deadman Bay rocks and also marks the top of an intensely faulted zone which varies in thickness from about 200 to 1000 m. This zone is dominated by meter-, dekameter-, and kilometer-scale slices of ribbon chert and minor pillow basalt of the Deadman Bay terrane. Slices of other units, unrelated to the subjacent Deadman Bay terrane, are typically restricted to the uppermost part of the fault zone. For instance, slices of Constitution Formation are generally confined to the uppermost 10 m of the zone. Dispersed within the upper 100 to 200 m of the fault zone are exotic meter- to dekameter-size slices of Garrison Schist, which consists of mafic and quartzose schists that were metamorphosed to greenschist- and albite-epidote amphibolite facies. Several K-Ar amphibole dates indicate a Permian and/or Triassic age for this metamorphism. The rocks within the fault zone, as well as the nappes above and below, record a regional high pressure-low temperature metamorphism characterized by widespread prehnite and aragonite, with minor lawsonite and aluminous pumpellyite.

The slices of Garrison Schist are found along much of the mapped extent of the Rosario fault (figures 3 and 13 in Brandon and others, 1988). These slices must represent an exotic component because they cannot be related to the present footwall or hangingwall of the Rosario fault zone. In other words, we cannot find a footwall or hangingwall cutoff

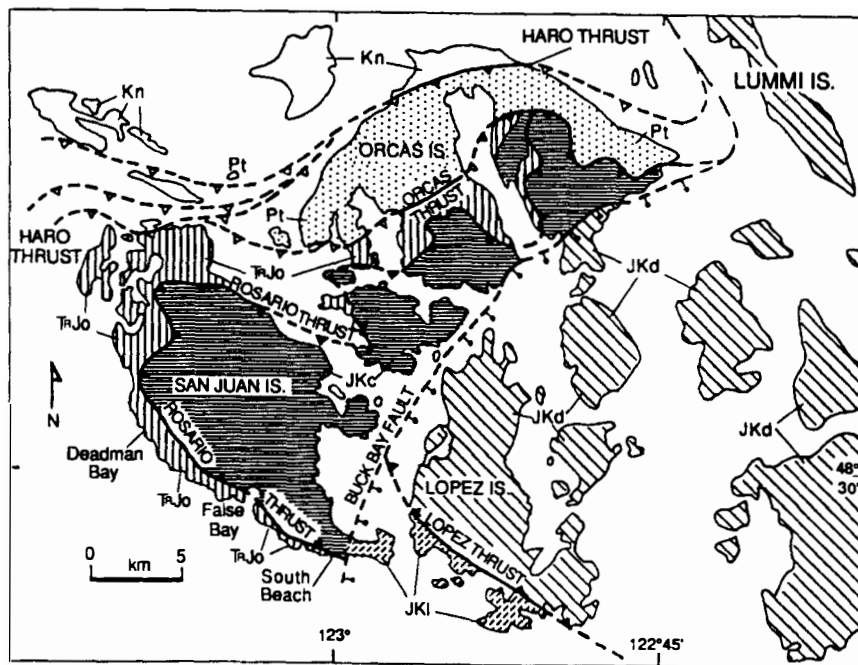


Figure 3. Generalized geology of the San Juan Islands showing the major large-slip thrusts: Haro, Orcas, Rosario, and Lopez. JKd = rocks of the Decatur terrane, constituting the hanging wall of the Lopez thrust. JKI = Lopez Structural Complex, composed of diverse structural slices within the Lopez fault zone. JKc = Constitution Formation, a nappe bounded above by the Lopez Complex and below by the Rosario thrust. TrJo = Orcas Chert and Deadman Bay Volcanics (Deadman Bay terrane) which collective make up the footwall of the Rosario thrust. Pt = Paleozoic Turtleback Complex and related rocks. Kn = Upper Cretaceous Nanaimo Group. The Buck Bay fault, which is inferred to dip to the southeast, may represent a younger normal fault. Map adapted from figures 3 and 5 in Brandon and others (1988).

from which the slices of Garrison might have been derived. Likewise, there is no apparent footwall cutoff from which the Constitution Formation in the overlying nappe was derived. Both of these relationships indicate that offset on the Rosario fault zone must exceed the present amount of structural overlap across the zone. This overlap requires a minimum of 30 km of slip for top-to-the-southwest transport and 18 km for top-to-the-northwest transport. The presence of the Garrison slices in the upper part of the zone suggests that much of this estimated minimum slip must have been accommodated in the upper 100 to 200 m of the fault zone. Thus, we consider the Rosario thrust and the uppermost part of the Rosario fault zone to mark the locus of a large-slip fault. Most of the distinctive fault-zone structures described herein are in this part of the Rosario fault zone.

Lopez Structural Complex

The Lopez Structural Complex (Figs. 3 and 18) is a 3-km thick, northeast-dipping fault zone lying beneath the Lopez thrust. The hangingwall is a relatively coherent nappe, the Decatur terrane, which encompasses the Fidalgo Igneous Complex, a Middle and Upper Jurassic ophiolite and volcanic arc, and overlying Upper Jurassic marine clastic strata of the Lummi Group. The footwall is the Constitution Formation. The Lopez Complex consists of imbricated lenticular slices that were mostly derived from adjacent hangingwall and footwall units. However, two exotic units are present. Lower Paleozoic tonalite and gabbro are found in two small (<150 m) fault slices. These rocks are equivalent to the Turtleback Igneous Complex which is mainly exposed in the northern San Juan Islands (20 km north of the Lopez Complex), where it forms one of the lowest nappes in the stack. Small fault slices of Turtleback Complex are distributed locally in other fault zones of the San Juan Islands (figure 3 in Brandon and others, 1988), but the slices in the Lopez Complex represent the structurally highest occurrence of this unit. The other exotic unit consists of uppermost Albian pillow basalts of Richardson, which are restricted to a 3 km-long slice in the Lopez Complex. Like the Garrison slices in the Rosario fault zone, we cannot find a footwall or hanging cutoff from which the basalts of Richardson might have been derived.

The minimum amount of slip across the Lopez fault zone can be estimated by considering the minimum distances required to restore the hangingwall and exotic fault slices back to their footwall sources. For the case of top-to-the-southwest transport, the nearest footwall source for the Turtleback Complex (easternmost tip of Orcas Island) indicates a minimum slip of 26 km. The absence of a footwall source for the basalts of Richardson gives a similar minimum estimate. These relationships cannot be used for the case of top-to-the-northwest transport because the Lopez zone lies at the southern outcrop limit of the San Juan nappes. The absence of a pronounced gravity anomaly over the Decatur terrane indicates that much of the mantle base of this ophiolitic nappe is probably missing. This relationship implies that the amount of slip on the Lopez fault must be greater than the dimensions of the Decatur nappe itself. This argument indicates a minimum slip of about 30 km, regardless of transport direction, because of the equant shape

in map view of the Decatur terrane (figure 3 in Brandon and others, 1988).

To summarize, the Lopez and Rosario fault zones are similar in two respects: (1) they both have accommodated large amounts of fault slip (>30 km), and (2) they both contain exotic fault slices. They are different, however, in several ways. For the Lopez Complex, (1) the fault zone is much thicker (3 km versus ~200 m), (2) fault slices of different parentage (i.e., hangingwall, footwall, or exotic sources) appear to be more evenly distributed within the zone, and (3) fault-related deformation appears to be less intense. These observations suggest that slip across the Lopez Complex was accommodated on a more evenly distributed system of faults, whereas slip across the Rosario zone was strongly localized at the top of the zone.

Deformational and Metamorphic History of the Rosario and Lopez Fault Zones

Brandon and others (1988, 1993) presented evidence for a well-defined sequence of deformation, metamorphism, and uplift between about 100 and 84 Ma in the San Juan Islands. The earliest event in this Late Cretaceous history was the juxtaposition of nappes along the Rosario, Lopez, and kindred large-slip fault zones (Fig. 3). This event is interpreted as no older than 100 Ma, on the basis of the latest Albian age of the youngest rocks in the Lopez Complex. The imbrication of fault slices and the transport of exotic blocks within these fault zones occurred in a deformational regime dominated by brittle microfracturing and cataclastic flow.

The entire thrust system, including nappes and fault zones, was subsequently affected by a very low-temperature, high-pressure metamorphism, recorded by the static growth of lawsonite, pumpellyite, prehnite, and aragonite (see Brandon and others, 1988, 1993, and Cowan and Brandon, 1994, for supporting petrographic evidence). For example, relatively undeformed veins of aragonite and lawsonite commonly overprint a pervasive cataclastic fabric found in most of the exotic fault slices, especially slices of Garrison Schist and Turtleback complex. This fabric is attributed to brittle deformation associated with the incorporation and transport of these blocks in the fault zones. We conclude that metamorphism must have postdated much, if not all, of the slip within these fault zones. Note that our conclusions differ from those of Maekawa and Brown (1991, 1993), who argued that metamorphism was synchronous with faulting. Metamorphic assemblages, together with apatite and zircon fission-track ages, indicate that peak metamorphic conditions for the Rosario and Lopez zones and adjacent nappes were in the range of 150° to 200°C and about 500 Mpa (5 kb).

After imbrication and peak metamorphism, a prominent SMT cleavage was locally formed. This cleavage is best developed on the southern parts of San Juan, Lopez, and Lummi islands. It generally dips moderately to the northeast. In thin section, the cleavage is defined by dark discontinuous selvages with a spacing of 100 to 200 μm . Detrital grains in sandstone commonly show overgrowths of straight fibers oriented parallel to the cleavage. These fibers mark the extension direction during cleavage formation. Where best studied in the southern San Juan Islands, the cleavage appears to postdate fault-zone deformation and high-pressure

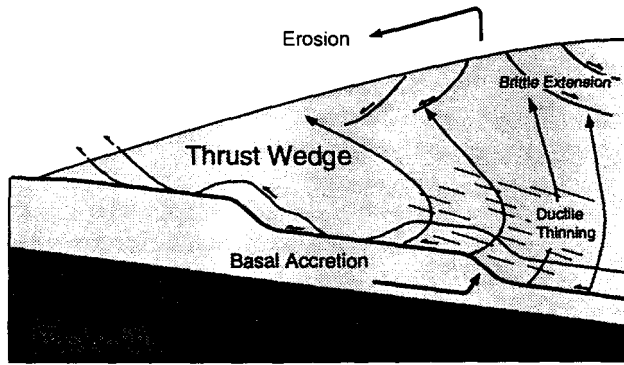


Figure 4. Schematic cross-section of a thrust wedge. Rocks undergo structural burial as part of the down-going plate. They are transferred by accretion to the base of the wedge where they begin their ascent to the surface. To exhume a rock from the base of the wedge, it is necessary to decrease the thickness of the overlying section. As illustrated in this figure, possible exhumation processes include: erosion at the top of the wedge, and thinning within the wedge by ductile flow or by normal faulting,

metamorphism in the Rosario and Lopez fault zones. For example, in many cases, the cleavage can be traced across specific faults, or from fault slices into a surrounding fault-zone matrix. Furthermore, we have found veins of lawsonite + pumpellyite that were shortened or extended depending on their initial orientation to the principal directions of cleavage-related strain (Cowan and Brandon, 1994).

Maekawa and Brown (1991, 1993) argued that this cleavage was formed by non-coaxial shear associated with fault slip. We disagree. Our observations indicate that the cleavage is a widespread regional feature and is not confined to individual fault zones. Furthermore, the straight fibers associated with the cleavage indicate that cleavage-related deformation was coaxial. We interpret this cleavage to have formed by late-stage ductile shortening within the thrust wedge after accretion of the nappes (Fig. 4).

We conclude that the high-pressure metamorphism and subsequent development of the cleavage are regional-scale events which occurred before 84 Ma. The best evidence for this timing is a Santonian conglomerate in the Upper Cretaceous Nanaimo Group (Figs. 1 and 3) that contains cobbles of lawsonite/pumpellyite-bearing sandstone closely resembling the metamorphosed Constitution Formation. Apatite fission-track ages from the San Juan Islands indicate cooling at ~87 Ma (Johnson and others, 1986; Brandon and others, 1988) and are compatible with the interpretation that the nappes were uplifted and erosionally unroofed during the Late Cretaceous.

In summary, the orogenic history of the San Juan nappes consisted of: (1) juxtaposition of nappes along the Rosario, Lopez, and related large-slip fault zones, (2) high-pressure metamorphism, (3) formation of cleavage, and (4) erosional exhumation. All of these events took place within a 16 m.y. interval (100 to 84 Ma), during which time the nappes traversed a round-trip vertical distance of about 36 km, at an average vertical rate of about 2 km/m.y. Brandon and others (1988) favor the interpretation that these events are collectively related to accretion of the San Juan nappes at a depth of about 18 km beneath an actively advancing orogenic wedge (Fig. 4).

On the basis of a kinematic analysis of mesoscale fault-zone structures, Cowan and Brandon (1994) concluded that regional slip on the Lopez and Rosario thrusts was top-to-the-south and southwest, respectively. These findings are compatible with the contractional model and are at variance with the top-to-the-north-northwest slip predicted by the transcurrent model (Maekawa and Brown, 1991).

Kinematic Analysis of Mesoscale Structures in Brittle Fault and Shear Zones

Cowan and Brandon (1994) described a method for synoptic analysis of kinematic indicators from brittle fault zones and applied the method to the Rosario and Lopez fault zones. Their method, which we call the internal-rotation axis (IRA) method, can be viewed as an extension of the slip-line method of Hansen (1971). The main difference is that the IRA method is directed towards resolving the symmetry of the deformation within the fault zone. As outlined by Paterson and Weiss (1961), the symmetry principle states that the symmetry of the final deformational fabric will include those symmetry elements that are common to the deformation and the initial fabric of rock. We assume that, on average, the deformation in a brittle shear zone has monoclinic symmetry, defined by a single mirror plane (Fig. 5). If correct, then we might expect to find this mirror plane as an element of the symmetry of the resultant shear-zone fabric, which is defined by the geometry and asymmetry of the structures and kinematic indicators within the shear zone. If the mirror plane can be determined, then its intersection with the shear plane gives the slip direction (Fig. 5).

The IRA method requires mesoscale structures that preserve information about the rotational component of the deformation. Examples are asymmetric folds and Riedel composite structures, both of which will be observed on the field trip. The term "Riedel composite structure", or Riedel

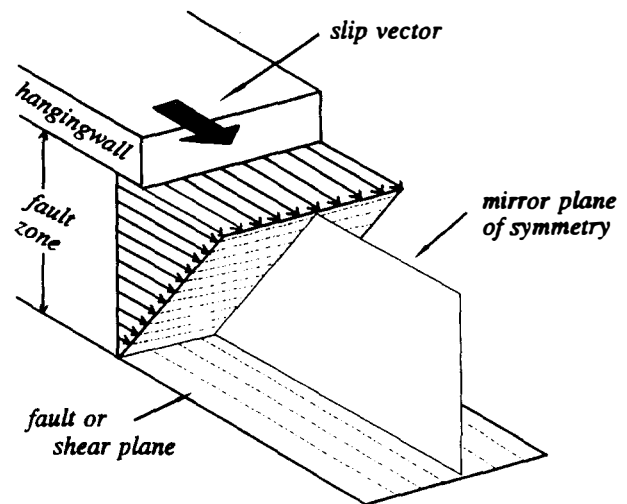


Figure 5. Idealized brittle shear zone illustrating the monoclinic symmetry of the average velocity field, assuming simple-shear deformation (adapted from fig. 1 in Twiss and Gefell, 1990).

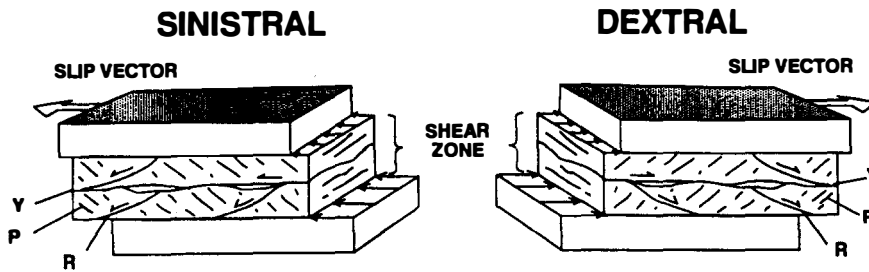


Figure 6. Block diagrams showing the geometry of two idealized Riedel structures: one is sinistral (top-to-the-left), and the other dextral (top-to-the-right). The primary slip surface is labelled Y. Secondary additive faults, which are inclined in the direction of slip, are labelled R. Surfaces inclined in the opposite direction, which might be shear fractures or penetrative foliations, are labelled P. In the Rosario fault zone, P is a cataclastic foliation, not a shear fracture.

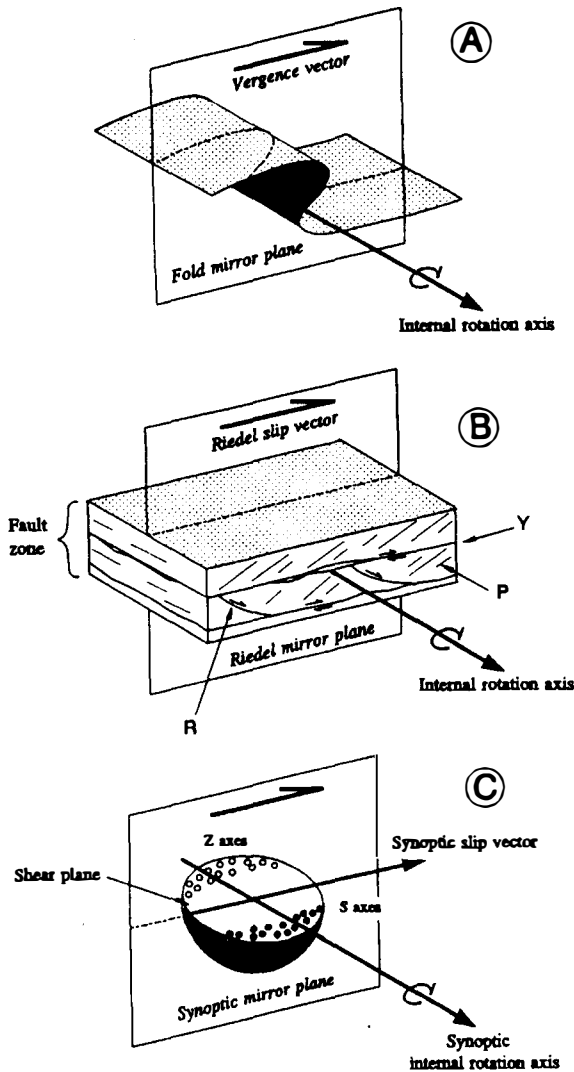


Figure 7. Internal-rotation axes are used to represent the orientation and asymmetry of (A) mesoscale folds and (B) Riedel composite structures. The stereogram in (C) illustrates a dispersion of individual internal-rotation axes about a mean direction, labelled as the synoptic internal-rotation axes. In the ideal case, this synoptic axis should lie normal to the mirror plane for a shear zone with monoclinic symmetry.

structure for short, refers to a distinctive array of contemporaneous planar structures (Fig. 6) that form during non-coaxial brittle shear in gouge-like materials (e.g., Logan

and others, 1979). Observations in both natural fault zones and experimentally produced brittle-shear zones indicate that slip can occur on all of the component surfaces, Y, R, and P, that make up the Riedel composite structure. Rutter and others (1986) and Chester and Logan (1987), among others, have also described instances where P corresponds to a penetrative foliation, which we refer to as a P-foliation. Riedel structures in the Rosario fault zone comprise Y and R slip surfaces and a P-foliation; P-slip

surfaces are not present.

Cowan and Brandon (1994) propose that the orientation and asymmetry of each fold or Riedel structure can be represented by an *internal-rotation axis* (Fig. 7). In theory, this axis correspond to the axis of shear-induced rotation (cf., Means and others, 1980) for the bulk deformation represented by the fold or Riedel structure. Because an internal-rotation axis is an axial vector, one must designate both a direction and a sense of rotation. The geologic convention is to use "S" and "Z" to indicate an anticlockwise and clockwise rotation, respectively, when viewed in the direction indicated by the axial vector. Note that S and Z are equivalent to "left-handed" and "right-handed" rotations, where the thumb is extended in the direction of the axis and the remaining fingers curl in the direction of rotation. An advantage of this convention is that all of the axes can be displayed in a lower-hemisphere stereogram. For an asymmetric fold, the internal-rotation axis is equivalent to the fold axis. For a Riedel structure, the internal-rotation axis is parallel to the intersection of the Y-surface with either R or P. The intersection is calculated from the attitudes of Y, R, and P measured in the field. The sense of rotation, S or Z, is inferred from the geometry of the structure (Fig. 7B).

In accord with the assumptions underlying the IRA method, Fig. 7C shows the hypothesized distribution of S and Z internal-rotation axes for a group of related structures produced in a fault zone. The axes all lie near a common plane, which parallels the attitude of the fault zone in which they formed. The monoclinic symmetry of the distribution is indicated by the single mirror plane, which lies perpendicular to the shear plane and bisects the two groups of S and Z axes. For this case, we infer that the *synoptic slip vector* for the fault zone lies at the intersection of the mirror plane and the plane of the fault zone. This vector can be viewed as the average direction of slip in the fault zone. In defining the slip vector, we use a footwall-fixed convention, that is, the slip vector corresponds to the direction of motion of the hangingwall relative to a fixed footwall.

The *synoptic internal-rotation axis* lies in the shear plane and is normal to the mirror plane. Note that in the schematic example given in Fig. 7C, the internal-rotation axes are dispersed around the synoptic axis. For real fault zones, internal-rotation axes commonly show a dispersed girdle

pattern, as first noted by Hansen (1971). Other types of patterns are also possible; for instance, Ring and Brandon (1994) describe dispersed cluster patterns for internal-rotation axes from the Coast Range fault of California. The cause of this dispersion remains poorly understood. It may reflect the actual mechanisms associated with slip within the fault zone, or may instead be due to random aspects of fault-zone deformation or to pre-existing structures in the fault zone.

To find the mirror plane, Cowan and Brandon (1994) plotted Z -transformed internal-rotation axes in a fault-parallel stereogram where the primitive circle of the stereogram is parallel to the fault plane. Z -transformed axes means that all axes have been converted to a common Z -sense of rotation. Note that, in general, the Z -transformed axes will include both lower and upper hemisphere directions. The average of the Z -transformed axes is considered to be the best estimate of the synoptic internal-rotation axis. Another approach, used by Ring and Brandon (1994), is to plot and contour the Z -transformed axes using both lower and upper hemispheres of the stereogram. This approach is useful for axis distributions that lack a girdle pattern. Furthermore, it does not require rotation of the axes into a fault-parallel stereogram. The stereograms can be constructed and analyzed in present geographic coordinates. The Fisher vector mean can be used to estimate the orientation of the synoptic internal-rotation axis.

SMT cleavage

There are several reasons for our interest in the SMT cleavage in the San Juan-Cascade nappes: (1) Kinematic information about the cleavage is useful in assessing various tectonic models for the San Juan-Cascade nappes (Fig. 2). For instance, Maekawa and Brown (1991, 1993) argued that this cleavage was formed by non-coaxial shear associated with horizontal dextral shear as specified in the transcurrent model, whereas Brandon and others (1988, 1993) and Cowan and Brandon (1994) argued that the cleavage recorded northeast-southwest shortening as predicted by the contractional model.

(2) The cleavage also provides information about deformational processes operating with a contractional wedge. For instance, Selverstone (1985), Platt (1986), and Wallis and others (1993), among others, have argued that ductile flow within a contractional wedge might cause vertical thinning within the upper part of the wedge and thus contribute to the exhumation of the metamorphic interior of the wedge. Because the exhumed rocks traversed the entire wedge, they preserve an integrated record of the strain field within the wedge.

(3) Finally, the cleavage may also preserve information about the fluid flow history of the wedge. Of particular interest is the volume strain

and mass loss associated with SMT deformation. A large loss of mass would require pervasive and prolonged fluid flow, given the low solubility of silicate minerals especially at temperatures $< 250^{\circ}\text{C}$.

For our strain study, we have focused on fine- and medium-grain sandstones because the detrital grains can be used as strain markers. Feehan and Brandon collected about 90 oriented samples in the Northwest Cascades and the San Juan Islands, with most of the samples focused on the Lopez Complex. Twenty-seven of these sample proved suitable for strain analysis (Fig. 1).

Cleavage is the only penetrative fabric present in these samples. In thin section, the sandstones show truncated detrital grains, discontinuous anastomosing selvages, and directed fiber overgrowths composed of quartz, chlorite, and phengite. Petrographic evidence indicates that the fibers were actively accreted at the grain boundary (e.g., pyrite-type of Ramsay and Huber, 1983, p. 265). Intragranular and transgranular fractures are relatively rare. First-cycle grains of volcanic quartz show no evidence of undulose extinction or subgrain formation, which indicates that the dislocation-glide mechanism was not operative. These textural observations indicate that SMT was the dominant deformational mechanism, with grains shortened by grain-boundary dissolution and extended by precipitation of directed fiber overgrowths. SMT is the expected mechanism given the relatively low temperatures attending deformation. The fact that the fibers are parallel to the selvages indicates that the deformation was approximately coaxial and that the cleavage did not form by simple shear as proposed by Maekawa and Brown (1991).

We have devised some new methods for measuring strain

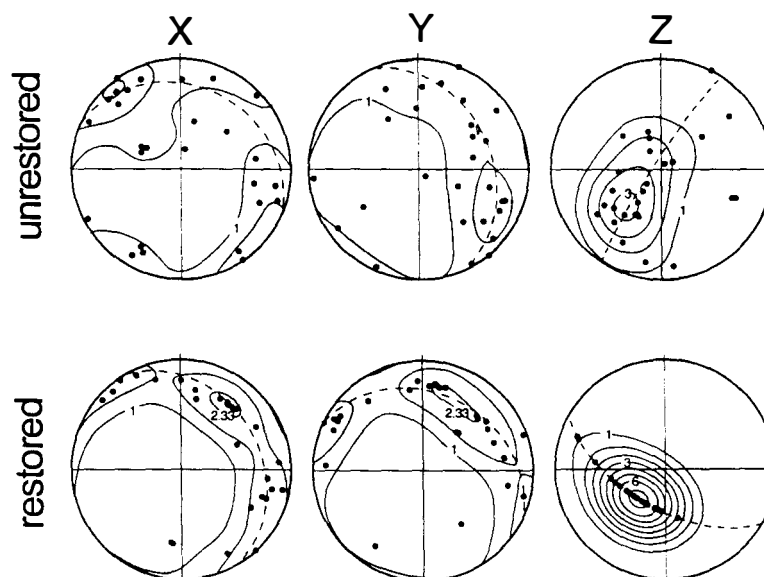


Figure 8. Equal-area stereograms of principal directions for strain data. X, Y, and Z indicate the maximum extension, intermediate and maximum shortening directions, respectively. Stereograms labelled "unrestored" show principal directions in their present orientations. Those labelled "restored" show directions after approximate correction for rotations due to Cenozoic folding (see text for details). Density contours are according to the method of Kamb (1959). Contours start at one times uniform density and increase in increments of 0.66 times uniform density. Areas with densities greater than 2 times uniform are considered to be significantly overpopulated.

TABLE 1. Strain data for the San Juan–Cascade nappes

No.	Sx			Sy			Sz			Sv		Modes (%)	
	Stretch, trend, plunge			Stretch, trend, plunge			Stretch, trend, plunge			V _t /V _i ± RSE(%) [*]		Fiber	Selvage
<i>Lopez Structural Complex, San Juan Islands</i>													
1	1.27	113	24	0.8	358	44	0.53	222	36	0.54	8.5	20.6	2.5
2	1.27	299	56	0.86	33	26	0.52	190	16	0.57	7.5	21.1	1.2
3	1.24	20	14	0.78	129	26	0.59	267	58	0.57	10.7	19.6	2.7
4	1.20	101	33	0.77	329	46	0.71	208	26	0.65	10.3	16.9	0.3
5	1.41	108	9	0.71	15	20	0.53	221	69	0.53	9.8	29	0.6
6	1.25	100	14	0.65	3	26	0.59	216	60	0.47	8.6	19.7	1.1
7	1.15	326	15	0.78	67	34	0.65	208	52	0.58	10.9	13.2	1.2
8	1.30	82	32	0.75	338	23	0.54	206	51	0.53	8.8	22.9	2
9	1.20	51	45	0.73	141	0	0.54	231	44	0.47	8.4	17.1	7.5
10	1.13	16	53	0.9	133	9	0.47	235	30	0.48	13.4	11.8	2.5
11	—	1	20	—	104	34	—	247	50	—	—	—	—
12	—	314	10	—	50	37	—	210	51	—	—	—	—
13	1.25	297	7	0.72	135	83	0.52	27	0	0.47	8.5	19.7	1.5
14	—	320	10	—	59	42	—	219	46	—	—	—	—
<i>Constitution, Lummi and Obstruction Formations, San Juan Islands</i>													
15	—	145	10	—	53	12	—	227	75	—	—	—	—
16	—	208	22	—	111	20	—	341	60	—	—	—	—
17	1.17	205	18	0.77	110	18	0.62	340	65	0.56	8.5	14.4	2.3
18	1.27	210	11	0.72	117	19	0.5	329	74	0.45	13.4	21	2.8
19	1.26	242	4	0.7	151	3	0.51	31	85	0.45	10.3	20.4	5.9
20	1.19	46	4	0.89	140	38	0.53	311	52	0.56	8.2	15.8	1
21	1.08	316	20	0.94	113	58	0.66	52	23	0.67	10.9	7.2	0.7
<i>Nooksack Formation, Northwest Cascades</i>													
22	1.32	146	1	0.75	236	39	0.49	51	51	0.48	11.7	24.5	1.3
23	—	325	0	—	234	10	—	55	80	—	—	—	—
24	1.08	12	75	0.81	265	5	0.67	173	13	0.58	8.5	7.3	1.5
25	1.26	336	12	0.79	78	48	0.55	238	39	0.55	10.7	19.7	1.5
26	—	301	60	—	204	4	—	111	29	—	—	—	—
27	—	292	58	—	22	0	—	112	32	—	—	—	—
TENSOR AVERAGE													
Unrestored	0.95	110	13	0.82	14	26	0.68	224	60	0.53	—	17	1.6
Restored	1.01	353	20	0.91	92	23	0.58	226	60	0.53	—	17	1.6

* RSE refers to the estimated relative standard error, reported as a percentage of the volume stretch.

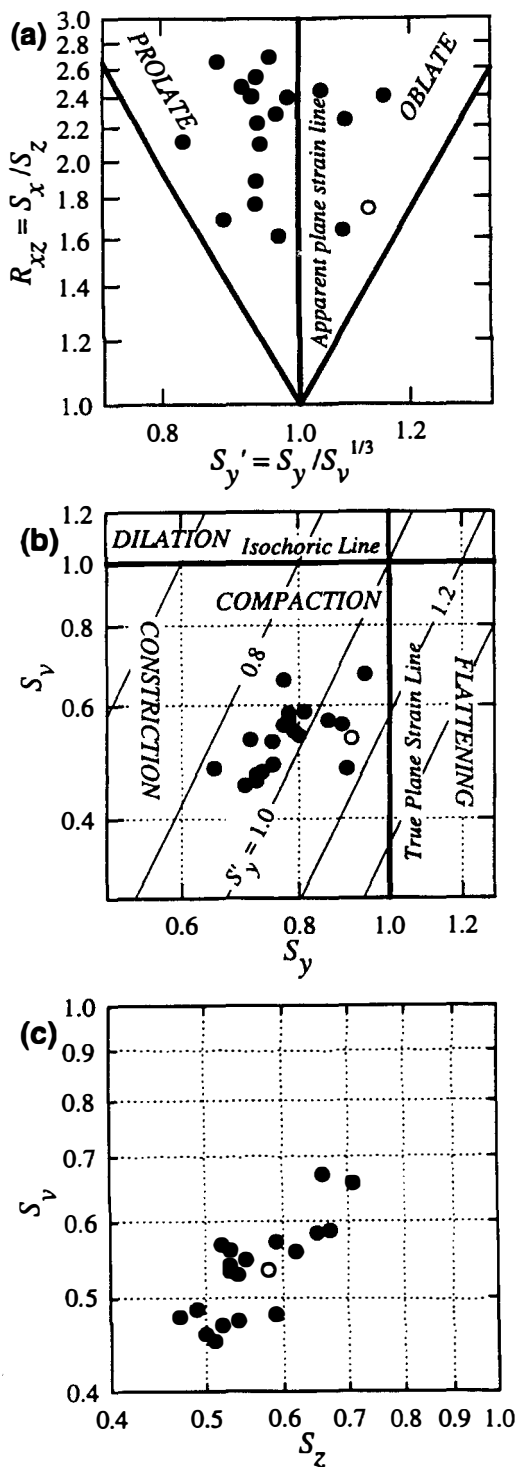
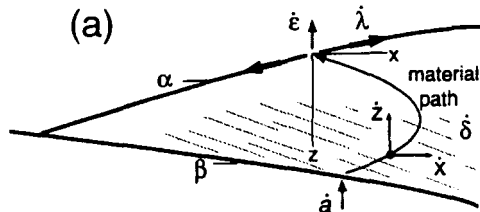


Figure 9. Plots of strain magnitude data (see Brandon, 1994, for details about construction of plots). The open symbol represents the tensor average for the restored data. (A) The modified Nadai plot is based on strain ratios and indicates the symmetry of the strain. (S'_y is the intermediate deviatoric stretch, equal to the intermediate stretch normalized to constant volume.) Note that the individual strain measurements generally have a prolate symmetry whereas the tensor average strain has oblate symmetry. (B) The strain-type plot, which is based on absolute magnitudes of the stretches, indicates that the strain is generally constrictional ($S_y < 1$) and involved a significant loss of volume ($S_v < 1$). The intermediate deviatoric stretch, S'_y , is indicated by the diagonal contours. (C) This plot shows that the volume stretch is primarily a function of shortening in the Z direction.

in these rocks. Traditional methods, such as the $R_x\text{-}\phi$ method, are not suitable because the grains do not deform as passive markers but rather by modification of their external shapes. The first step is to determine the principal directions for SMT strain, X, Y, Z, corresponding to the maximum extension, intermediate, and maximum shortening directions, respectively. The cleavage plane is assumed to lie perpendicular to Z. To determine the X direction, we measure the average orientation of the directed fiber overgrowths in an XY thin section cut parallel to cleavage. Y is then defined by its orthogonality with X and Z. With this information, we make an XZ thin section. For each sample, both the XY and XZ sections showed well organized fiber overgrowths oriented in the same direction. Therefore, the maximum extensional stretch S_x is related to the modal abundance of fiber by the following relationship: $S_x = 1/(1-m)$ where m is the modal fraction of fiber. (Stretch is defined as $S = \text{final length} / \text{initial length}$.) Modes are determined using an automated micron-stepping microscope.

Because the fibers only grow in one direction, we infer that the other two principal stretches, S_y and S_z , are less than or equal to one. To measure these stretches, we use the projected dimension strain (PDS) method. The idea behind this method is that the average projected dimension of the grains in the Y and Z directions must be reduced proportional to the principal stretches S_y and S_z , respectively. The projected dimension is also called the caliper dimension and corresponds to the size determined by placing the grain in a caliper scale with the direction of interest oriented perpendicular to the inside faces of the caliper. The initial average caliper dimension of the grains is preserved in the X direction because the grain is internally undeformed and the grain boundary in this direction is mantled by the fiber overgrowths. Therefore, the stretches in Y or Z should be equal to the average caliper dimension in Y or Z, respectively, divided by the average caliper dimension in X. These measurements are made in two dimensions, so we need to make a small conversion to get the correct three-dimensional result. We have tested the PDS method using undeformed sandstones and found that it is relatively insensitive to grain fabrics that might be produced during deposition and compaction. Therefore, the PDS method is considered to provide a direct measure of the strains resulting from the SMT mechanism.

Our measurements are reported in Table 1 and illustrated in Figures 8 and 9. The highlights are briefly itemized here. (1) The Z directions show a girdle pattern with a pole that plunges gently to the southeast (Fig. 8). We infer that this pattern is related to the development of broad long-wavelength folds during the Cenozoic. This folding event is well documented in Upper Cretaceous and Eocene strata to the north and east of the San Juan Islands, and in the broadly folded form of the thrust faults in the San Juan Islands (Fig. 3). To restore the effects of this post-orogenic folding, we have rotated the principal directions for each sample back around a common southeast-plunging fold axis by an amount sufficient to return the Z axis for the sample as close as possible to the average Z direction (Fig. 8). In Table 1 and Figures 8 and 9, this unfolded dataset is called



THINNING AND THICKENING RATES

- \dot{a} accretion
- $\dot{\delta}$ ductile flow
- $\dot{\lambda}$ shallow faulting
- $\dot{\epsilon}$ erosion

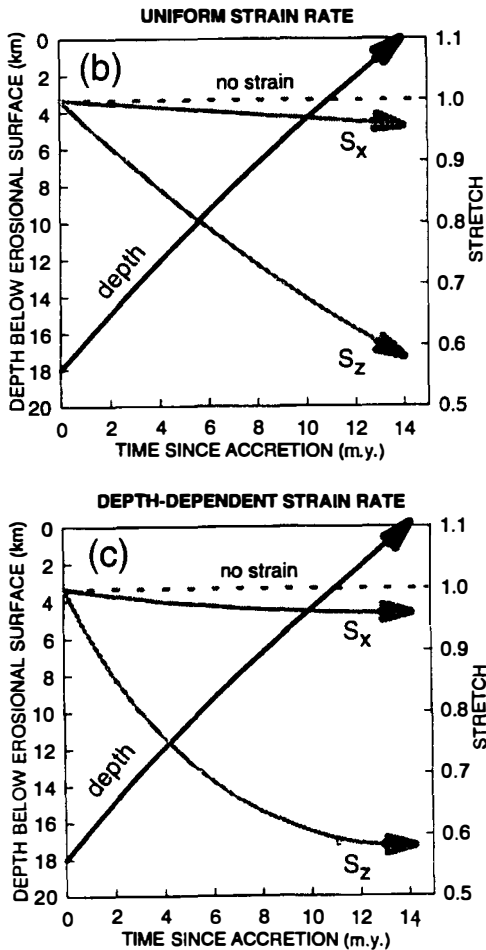


Figure 10. (A) Schematic cross section of an accretionary wedge showing the major processes causing vertical thinning or thickening and how they effect the exhumation of a particle moving through the wedge. For our model, these processes are represented as accretion at the base of the wedge, ductile flow within the wedge, and normal faulting and erosion causing thinning near the top of the wedge. The horizontal and vertical components of the velocity of the particle are indicated by \dot{x} and \dot{z} , respectively. (B) and (C) show the exhumation and strain history for a particle accreted at a depth of 18 km beneath a steady-state wedge and exhumed at the surface of the wedge after 14 m.y. Ductile strain accumulates as the particle moves through the wedge. (B) and (C) are based on rate laws for ductile flow that are uniform and proportional, respectively, with depth. The rate law is adjusted until the final ductile strain of the exhumed particle is equal to the average ductile strain determined in our study. The evolution of the principal stretches are shown by the curves labelled S_x and S_z . These calculations indicate that ductile strain contributed ~15 percent to the total exhumation.

“restored”.

(2) Both the unrestored and restored data show considerable variability for the X and Y directions and less variation for the Z directions (Fig. 8). The Z directions, on average, plunge moderately to the southwest, which is consistent with southwest–northeast orogenic shortening.

(3) The measured principal stretches indicate that the local strains have a prolate symmetry (Fig. 9a) and are weakly constrictional ($S_y < 1$; Fig. 9b). The largest distortion is associated with shortening in the Z direction (Fig. 9c). Strains in the Z direction range from –29 to –53 percent. Strains in the X and Y directions range from +8 to +41 percent and –6 to –35 percent, respectively.

(4) Volume stretch, S_v , equal to final volume / initial volume, can be estimated from the principal stretches by: $S_v = S_x S_y S_z$ (Table 1). Our results, when cited as volume strains, indicate a volume loss of 33 to 55 percent. Because the PDS method measures changes in the shapes of grains, we consider this estimate of volume loss to represent a loss of mass from the grains themselves.

(5) Table 1 shows the tensor average for our strain determinations using the method of Brandon (1994). The tensor average accounts for the fact that strain data include both magnitudes and directions. The tensor average should provide a better estimate of the regional strain by averaging out the local variations of the strain field and the errors in our strain measurements. The most interesting result is that none of the principal stretches is significantly greater than one. In other words, there is no evidence for any extension at the regional scale during SMT deformation.

On the basis of relative strain measurements, Maekawa and Brown (1991) argued that the San Juan–Cascade nappes were extended parallel to the strike of the orogen, which they took as evidence for transpressive shear. We note that our absolute strain measurements indicate an SMT strain of only –5 percent parallel to the strike of the orogen (~130°). In a horizontal direction across the orogen, SMT strain is –22 percent, which is consistent with other evidence for southwest–northeast orogenic contraction.

Our measurements indicate that SMT deformation resulted in shortening in the vertical, about –36 percent. To properly estimate the contribution that this process made to the total exhumation of the San Juan–Cascade nappes, we need to consider both the vertical rate at which the nappes moved through the wedge and the rate of thinning of the remaining overburden at each step along the path. Figure 10 summarizes the results of a one-dimensional model involving a single trajectory through a steady-state wedge (Fig. 10a). The rates of basal accretion, ductile strain, normal faulting, and erosion all remain constant with time. The particle is first accreted at a depth of 18 km, and then moves through the interior of the wedge where it accumulates ductile strain, and then reaches the surface 14 m.y. later. We allow 2 m.y. for subduction beneath the wedge, bring the total duration between subduction and exhumation to 16 m.y. To solve for the best-fit parameters, we iterate the model and search for parameters that give the correct amount of exhumation and finite strain after 14 m.y. Our model calculations have used a ductile-strain-rate law

that is either uniform (Fig. 10b) or proportional (Fig. 10c) with depth. These models indicate that ductile strain contributed about 19 percent (uniform rate) to 13 percent (proportional rate) to the overall exhumation. The other ~85% of the exhumation, equal to ~15 km, was due to shallow normal faulting or erosion. We suspect that erosion may have been the dominant process because we see no evidence of horizontal extension in the ductile strain nor have any large normal faults been identified within the San Juan-Cascade nappes. Furthermore, a record of erosional unroofing is clearly present in the Nanaimo basin. The required rates of erosion, ~1 km/m.y., are not unusual for an orogenic setting.

Road Log

Rather than use a conventional road log with mileages, we have found it to be more efficient to rely on a general map (Fig. 11) and detailed directions. The island roads are well marked, and the field stops are generally easy to find because they are located along the coastline. Transportation to the San Juan Islands is provided by Washington State Ferries; obtain schedules by telephoning (206) 464-6400. To reach the ferry terminal in Anacortes, drive north on I-5 from Seattle to exit 230, then drive west on SR 20. The driving

distance from downtown Seattle to Anacortes is ~80 miles.

Day 1. San Juan Island

Take the ferry to Friday Harbor on San Juan Island. Drive southwest from Friday Harbor for 1.7 miles on San Juan Valley Road. Turn south on Douglas Road and continue for 1.4 miles to the L-intersection with Bailer Hill Road. Turn right (west) and proceed for 5.5 miles on Bailer Hill Road and its continuation as West Side Road along the coast. Stop and park where West Side Road switches back and turns sharply east. This location is called Deadman Bay and is flanked to the north by Lime Kiln Park. Do not follow the gravel road to the west into park. Instead walk southwest along a series of footpaths to the rocky coastal exposures along the north side of Deadman Bay. Aim for the rocks just below and southeast of the whale-watching display.

Stop 1-1. Deadman Bay. The purpose of this stop is to examine the lower plate of the Rosario thrust and to discuss the overall structural setting of the San Juan thrust system. The following description is reproduced, with minor modifications, from field guides by Brandon and Cowan (1987) and Brandon (1989). This stop lies at the southern end of a 4-km-long fault-bounded slice of Deadman Bay

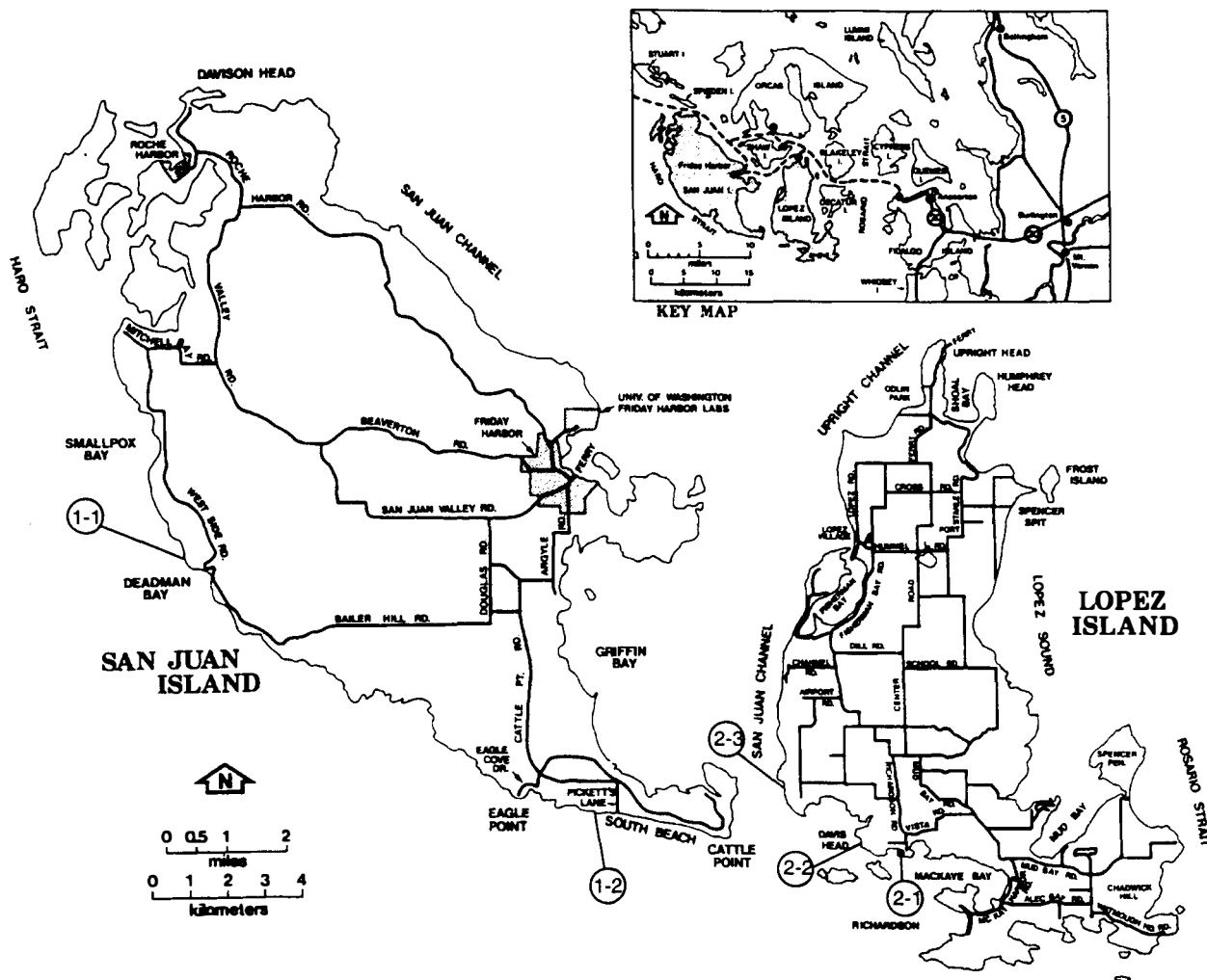


Figure 11. Roads and ferries in the vicinity of the San Juan Islands. Numbers show field stops.

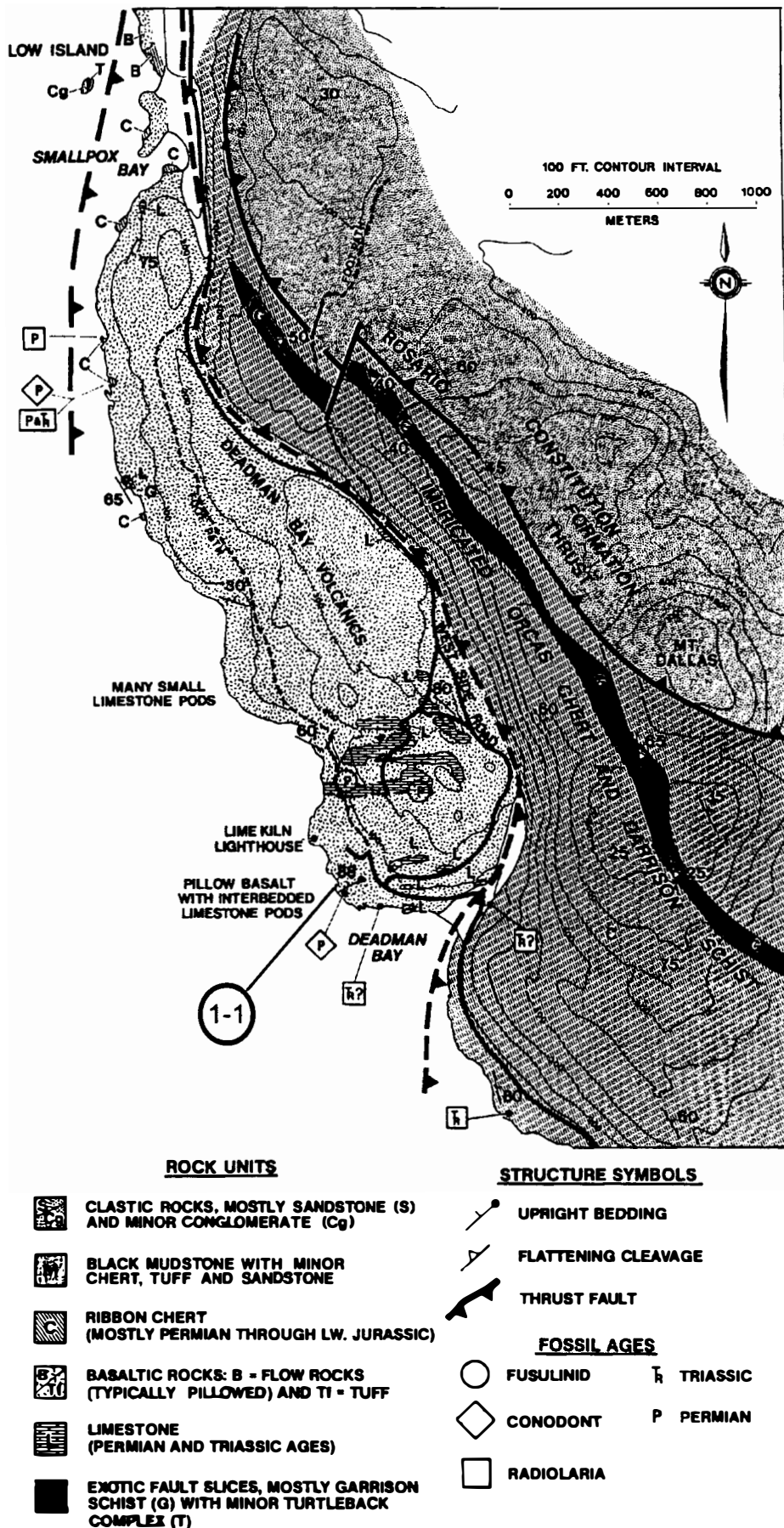


Figure 12. Geologic map for Stop 1-1 showing a large fault slice of Deadman Bay Volcanics on the west coast of San Juan Island. Map is from Brandon and others (1988); fossil localities are described there.

Volcanics (Fig. 12). Gray and green ribbon chert exposed at the south side of the bay belongs to the Orcas Chert, which structurally overlies the volcanics along a northeast-dipping thrust fault. Together, the Orcas Chert and Deadman Bay Volcanics constitute the Deadman Bay terrane (Fig. 3), which lies structurally beneath the Rosario thrust. Looking west, you can see Vancouver Island, much of which is underlain by the Wrangellia terrane (Fig. 1).

The Deadman Bay Volcanics are well exposed along the coast on the rocky headlands between the bay and the lighthouse to the north. The unit is dominated by red and green pillow basalt, breccia, and tuff with subordinate interbedded limestone. It is disrupted in many places by faults, but it generally has a persistent easterly strike and, in this area, a near-vertical dip. Geopetal structures indicate younging to the north. Limestones in the unit are massive and gray, and they contain small amounts of intercalated green tuff. Bedding, where present in the limestones, is typically contorted and appears to have been deformed by soft-sediment slumping. Carbonate material occurs interstitially in the pillow flows and might have been sucked into the pillowed framework by rapidly convecting currents generated by the cooling submarine flows or by churning as the lavas flowed across carbonate accumulations. Some of the limestones were converted to aragonite marble during Late Cretaceous high-pressure metamorphism.

Crinoid debris and fragments of other fossils can be found in many limestone pods. A thin limestone bed, clearly interbedded in the pillow basalt sequence at Deadman Bay, has yielded late Early Permian (late? Leonardian) conodonts (conodont locality at south end of map in Fig. 12). Limestone in a nearby quarry has yielded early Late Permian

(early Guadalupian) fusulinids (fusulinid localities at south end of map in Fig. 12). These fusulinids are Tethyan, which suggests that the Deadman Bay Volcanics are exotic to North America. Trace-element chemistry (high TiO₂ and light rare-earth element enrichment) indicates that the volcanics were probably erupted in an "oceanic-island" setting.

The Wrangellia terrane is interpreted to lie structurally beneath the Deadman Bay terrane—several kilometers below where we are standing. The bounding fault, the Haro thrust, marks the leading edge of the San Juan-Cascade nappes (Fig. 3) and must lie to the west beneath Haro Strait which separates the San Juan Islands from Vancouver Island. Note that much of the Wrangellia terrane is coeval with the Deadman Bay terrane but Wrangellia has a completely different stratigraphic and metamorphic history.

To reach Stop 1-2, drive 5.5 miles back along West Side Road and Bailer Road to the L-intersection with Douglas Road. Turn left (north) on Douglas Road, proceed for 0.5 miles, and then turn right (east) on an unnamed road. Proceed 0.5 miles to a T-intersection with Cattle Point Road. Turn right (south) on Cattle Point road, and proceed 3.9 miles to the intersection with Pickett's Lane. Turn right (south) on Pickett's Lane, and drive 0.5 miles to the parking lot at South Beach. Walk along South Beach to the first outcrop west of the beach.

Stop 1-2. Mesoscale structures and fault rocks in brittle shear zones in the Rosario thrust. This stop encompasses shoreline exposures extending approximately 400 m west of South Beach (Fig. 13). The entire stop is in San Juan Island National Historical Park, administered by

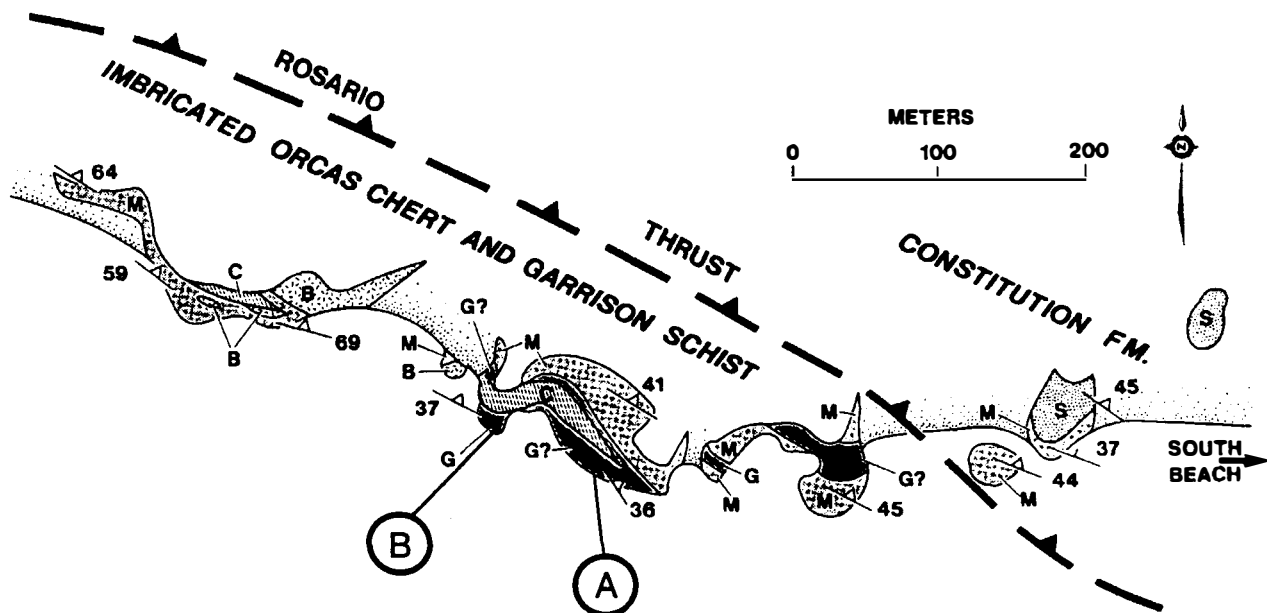


Figure 13. Outcrop map for Stop 1-2 showing the internal structure of the imbricate zone beneath the Rosario thrust at South Beach, southern San Juan Island (from Brandon and others, 1988). Locations A and B show exceptional exposures of mesoscale structures within the fault zone. Patterns and symbols are defined in Figure 12. Massive sandstone (S) and mudstone (M) of the Constitution Formation lie above the Rosario thrust. The area southwest and below the thrust consists of an imbricated fault zone containing ribbon chert (C) and pillow basalt (B) of the Orcas Chert, and small exotic fault slices of Garrison Schist (G).

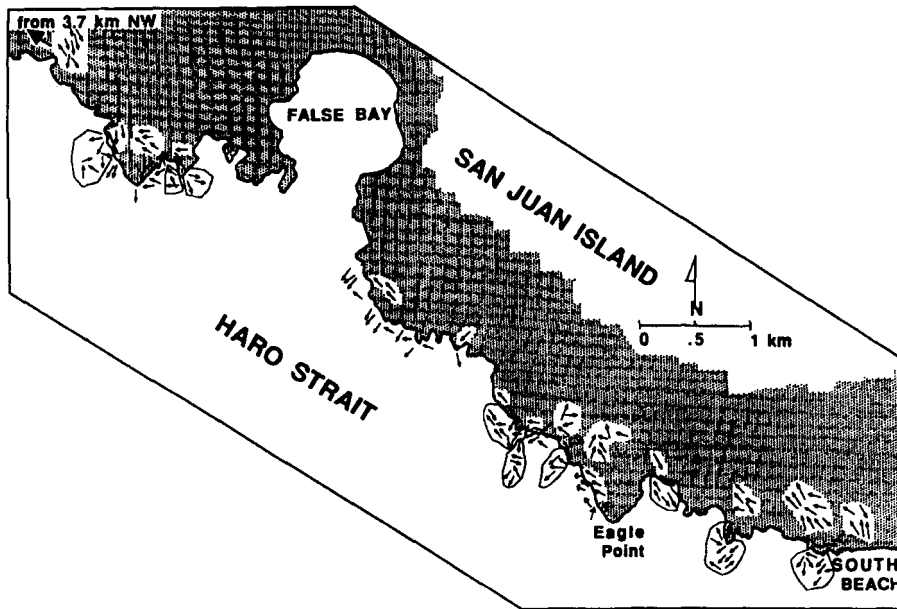


Figure 14. Map depicting the trend of local vergence vectors for folds (arrows plotted offshore) and slip vectors for Riedel structures (arrows plotted on land) in the Rosario fault zone. These structures are plotted stereographically in Figures 15 and 16. This figure illustrates the large angular dispersion among the individual kinematic indicators. A vergence vector, as used here, is perpendicular to the local fold hinge, parallel to the shear plane (G_f in Fig. 16), and points in a direction consistent with the sense of shear implied by the fold, assuming a footwall-fixed convention. Single-headed and double-headed arrows represent asymmetric and ambiguous folds, respectively. Where several measurements were made at one outcrop, the arrows are shown in a circled group.

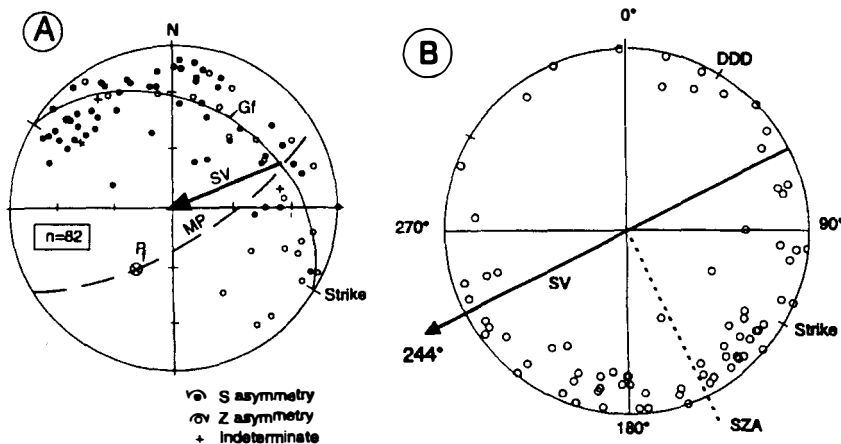


Figure 15. Synoptic analysis of mesoscale folds in the Rosario fault zone. (A) Lower-hemisphere stereogram of internal-rotation axes in present geographic orientation. G_f = average girdle for the fold axes. P_f = pole to G_f . M_p and SV are the inferred mirror plane and slip vector, respectively. (B) Fault-parallel stereogram showing Z-transformed axes. G_f was used to determine the rotation. SZA is the best-fit synoptic Z axis.

the National Park Service. Although this is public land, **collecting samples without a special collecting permit is illegal and prohibited. Leave your rock hammers in the car.** The following description is adapted in part from Brandon and Cowan (1987), Brandon (1989), and Cowan and Brandon (1994).

The outcrops at Stop 1-2 lie at the southeast end of the

trace of the Rosario thrust zone, which extends offshore beyond this point. The thrust dips northeast here, placing massive sandstone of the Constitution Formation over a structurally complex assortment of mudstone, green volcanic rocks (locally pillowed), green tuff, and ribbon chert, which are collectively assigned to the Orcas Chert (Deadman Bay terrane; see Brandon and others, 1988). The best evidence for large thrust displacements across the fault is the presence of exotic slices of Garrison Schist lying within the fault zone. The Garrison is a thoroughly recrystallized rock that was metamorphosed under greenschist and amphibolite conditions during the Permian and Triassic, long before its tectonic emplacement along the Late Cretaceous Rosario thrust (Brandon and others, 1988).

The easternmost outcrops in Figure 13 belong to the Constitution Formation (labeled "M" and "S") and

consist of a northeast-dipping depositional sequence that includes a thin horizon of mudstone, green tuff, and ribbon chert, overlain by a thick massive sandstone unit. Of particular interest is the clear interbedding of clastic rocks with radiolarian-bearing ribbon chert.

Farther west along the coast is a highly imbricated sequence of Orcas Chert with exotic slices of Garrison Schist. These rocks lie beneath the Rosario thrust, which is the highest recognized thrust within this imbricated fault zone. Here, and elsewhere in the San Juan Islands, the slices of dark- to light-green Garrison Schist are localized in a 100- to 200-m thick zone beneath the Rosario thrust. The

Garrison in the South Beach area is a brecciated to cataclastic, fine-grained mafic schist consisting of chlorite + actinolite + epidote + plagioclase.

The Orcas Chert and Garrison Schist in the outcrops along the coast display a variety of deformational styles. Some of the deformation was disorganized and chaotic, involving irregular mesoscale cataclastic flow of diverse rock types.

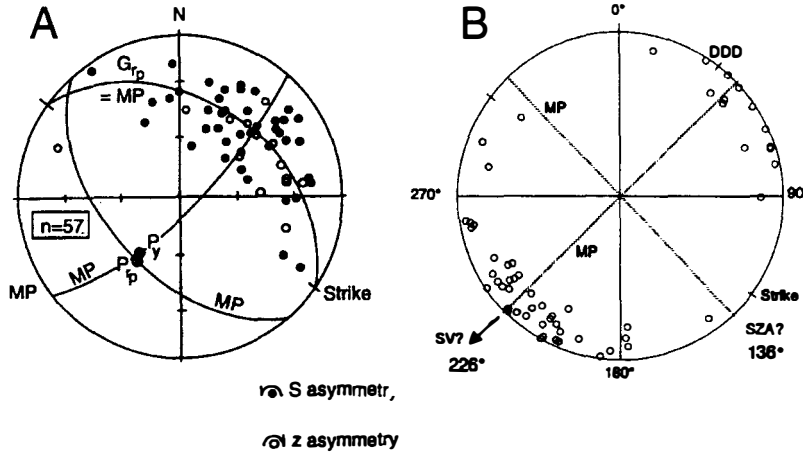


Figure 16. Synoptic analysis of Riedel structures in the Rosario fault zone. (A) Lower-hemisphere stereogram of internal-rotation axes in present geographic orientation. G_p = average girdle for the Riedel internal-rotation axes. P_p = pole to G_p . P_y = average pole for the Y surfaces. Note that the poles P_p and P_{ip} are nearly parallel as would be expected given the geometry of the Riedel structure. MP marks the three mirror planes inferred to be present in this subfabric; the slip vector is ambiguous. (B) Fault-parallel stereogram showing Z-transformed axes. G_p was used to determine the rotation. SZA? and SV? mark one possible interpretation for the orientations of the synoptic Z axis and the slip vector, respectively.

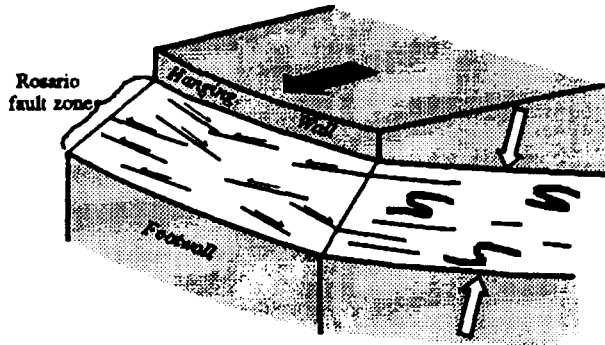


Figure 17. Schematic illustration of structures in the Rosario fault zone, as viewed from the south. We inferred a zone of general shear that was formed by: (1) top-to-the-southwest slip (large solid arrow) as recorded by southwest-verging asymmetric folds, and (2) shortening normal to the fault zone (two large open arrows) which resulted in two sets of opposed Riedel structures with average slip directions parallel to the strike of the fault zone.

Two exposures, however, display two types of mesoscale fault-related structures that Cowan and Brandon (1994) analyzed to deduce the regional slip vector along the Rosario thrust: Exposure A in Fig. 13 shows asymmetric folds, and Exposure B exhibits Riedel structures.

Exposure A is a steep rocky face along the coast. One or two meters below the top of the cliff, layers of chert interbedded with black mudstone locally display asymmetric folds. Folds in the Rosario fault zone indicate variable vergence directions, as shown in Figure 14 which covers the coast for some 12 km north of Stop 1-2. When these data are plotted stereographically (Fig. 15), the internal-rotation axes (equivalent to the fold axes) define a girdle pattern oriented subparallel to the fault zone. The synoptic Z axis (SZA in Fig. 15) indicates a top-to-the-southwest sense of

transport(250°, present coordinates) for the Rosario thrust.

Exposure B is a ~30 meter-wide headland. A 2 meter-high by 5 meter-long tectonic slice of green Garrison Schist crops out here, surrounded top and bottom and on the north by deformed mudstone and chert of the Orcas Chert. The schist has been almost completely pulverized into breccia and fine-grained cataclastite. Note that slickensides are generally not present in the Rosario fault zone. Those we have observed appear to be related to slip on the Y-shears of the Riedel structures. This fault-related fabric is cut by veins of aragonite produced during the regional high-pressure metamorphism (Cowan and Brandon, 1994). At the base of the inclusion, beneath the prominent overhang of schist, one can observe a zone of cataclastic flow, a few centimeters thick, in which green cataclastite derived from the schist was

mixed with black cataclastite derived from the mudstone.

Riedel structures are well developed in the deformed chert and mudstone for several meters structurally beneath and south of the inclusion, and locally elsewhere on the headland. Especially evident here are Y- and R-shears. The local slip vectors defined by the Riedel structures show a wide variation in directions, as illustrated in Figure 14. Figure 16b shows that the distribution of Z-transformed internal-rotation axes have two antipodal modes which indicates an orthorhombic symmetry for this component of the fault-zone fabric. Cowan and Brandon (1994) suggested that the Riedel structures formed by shortening normal to the fault zone (Fig. 17). This interpretation would imply that the brittle deformation within the fault zone that gave rise to asymmetric folds and Riedel structures is a result of general shear, combining top-to-the-southwest slip and northeast-southwest fault-normal shortening.

Note that here and at the previous exposure—in fact, in the Rosario thrust in general—striations are uncommon. We interpret those few that can be observed as having developed during slip on Y-shears in Riedel structures.

Day 2. Lopez Island

The Lopez Ferry Terminal is at the north end of the island, and our first stop is at the south end of the island at the community of Richardson. Drive 2.3 miles south on Ferry Road to the T-intersection with Lopez Road. Turn left (east) on Lopez Road and proceed 0.25 miles to the T-intersection with Center Road. Turn right (south) on Center Road and proceed 10.5 miles to the next T-intersection. Turn right (west), go 0.2 miles, and make your next left (south) on Richardson Road. Proceed 1.7 miles to where Richardson Road meets the coast. Park in the cul-de-sac.

Stop 2-1. Fault slice of exotic basalt in the Lopez Complex. Richardson is located in the Lopez Structural Complex (Fig. 18), a 2.5 km thick, northeast-dipping imbricate fault zone separating two more coherent Mesozoic units: the Decatur terrane in the hanging wall and the Constitution Formation in the footwall. At map scale, the Lopez Complex consists of an imbricated series of elongate, lenticular fault slices, which dip moderately northeast beneath the Decatur terrane. Many of the fault slices are similar to, and were probably derived from the Constitution Formation and Decatur terrane; others contain exotic units that cannot be related to rock units in the footwall or the hangingwall. These exotic units are lower Paleozoic tonalite of the Turtleback Complex, and the middle Cretaceous basalt, which is the focus of this stop.

The basalts of Richardson are part of a single fault slice about 2.5 km long and 275 m thick. The base of the slice will be examined at Stop 2-2. The slice consists "oceanic island" pillow basalts with minor pillow breccia, gabbro, tuff, and mudstone. The brownish-red mudstone bed in the 3-m-high roadcut at the north edge of the cul-de-sac has yielded the youngest fossils from the San Juan nappes. Foraminifera from these mudstones, first discovered by Danner (1966), have been identified as latest Albian (mid-Cretaceous, about 100 Ma). The slice of Richardson basalt is "exotic" because there is no footwall or hangingwall cutoff, along the traces of the thrusts bounding the Lopez Complex, from

which it could have been derived. The minimum slip across the Lopez Complex is about 25 km.

To reach Stop 2-2, drive north 0.25 km from the cul-de-sac at Richardson and turn left (west) on a gravel road. This road forks at 0.5 km. From this point on, you are on private property (Davis Head). Drive or walk on the right (north) fork. In 0.4 km, the main road turns left and uphill. Continue straight on the other road for 0.3 km and then turn left (south) and park. Walk south on a path to an open grassy area and then to the top of a steep brushy slope. Descend about 15 m on a footpath to a small gravel beach. This beach is privately but communally owned by the residents of Davis Head.

Stop 2-2. Mesoscale brittle-shear-zone structures and superposed SMT cleavage in the Lopez Structural Complex. Here we will examine diverse but representative fabrics and features that formed during imbrication of the Lopez Complex. First, turn northwest and walk along the base of the high rocky cliff. The cliff is made up largely of volcanic rocks, which, on the basis of their geochemistry, are correlated with the Richardson slice seen at Stop 2-1 (Fig. 18). At this stop, the base of the slice is a completely exposed brittle shear zone along which the volcanic rocks were emplaced over sedimentary rocks (sandstone, mudstone, conglomerate). The original volcanic features are

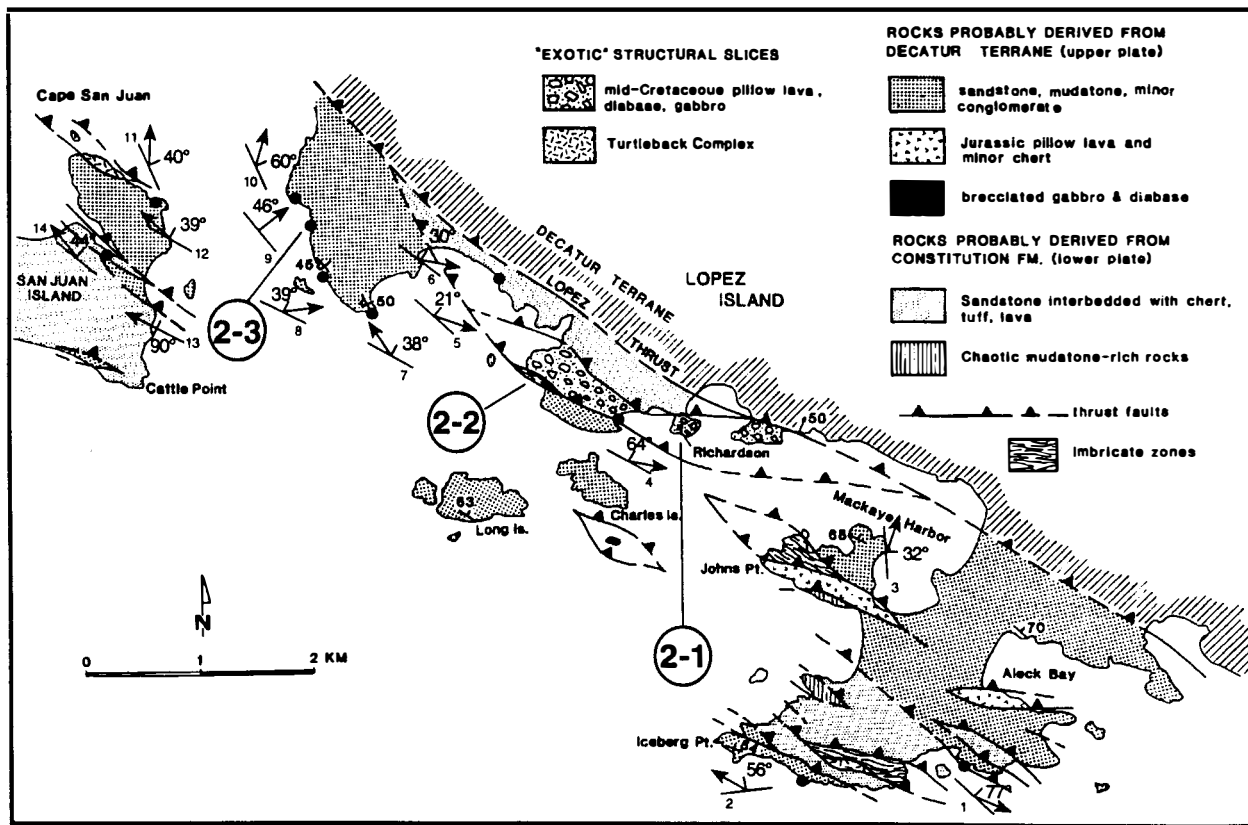


Figure 18. Geologic map for Stops 2-1, 2-2, and 2-3 showing the internal structure of the Lopez Structural Complex, exposed on the southern perimeter of Lopez and San Juan Islands (from Brandon and others, 1988). All contacts are faults. The large foliation/lineation symbols indicate the orientations of SMT strain data reported in Table 1: the foliation attitude is the flattening plane of the strain ellipsoid and the arrow indicates the trend of the maximum extension direction. The small foliation symbols show bedding attitudes in stratified units.

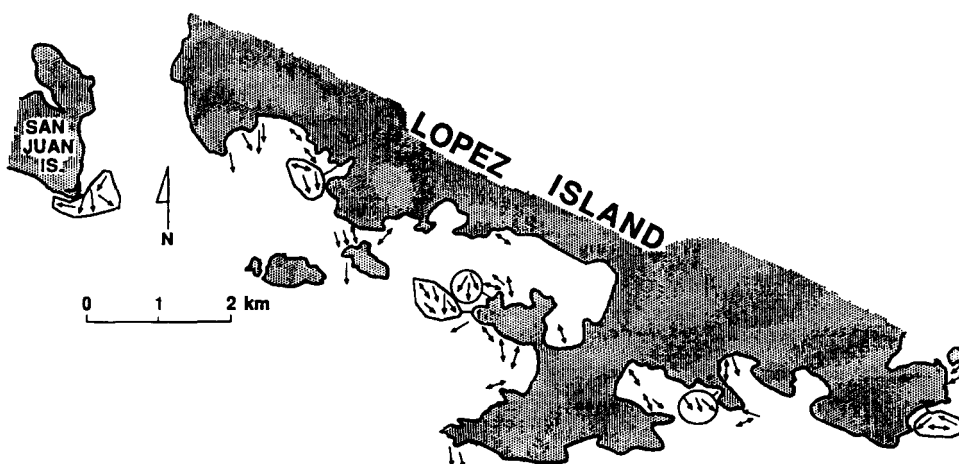


Figure 19. Map showing the trend of vergence vectors for mesoscale folds in the Lopez Complex. The same folds are plotted stereographically in Figure 20. This figure illustrates the large angular dispersion among the individual kinematic indicators. A vergence vector, as used here, is perpendicular to the local fold hinge, parallel to the shear plane (G_f in Figure 20), and points in a direction consistent with the sense of shear implied by the fold, assuming a footwall-fixed convention. Single-headed and double-headed arrows represent asymmetric and ambiguous folds, respectively. All arrows are plotted offshore, adjacent to coastal outcrops where the folds were measured. Where several measurements were made at one outcrop, the arrows are shown in a circled group.

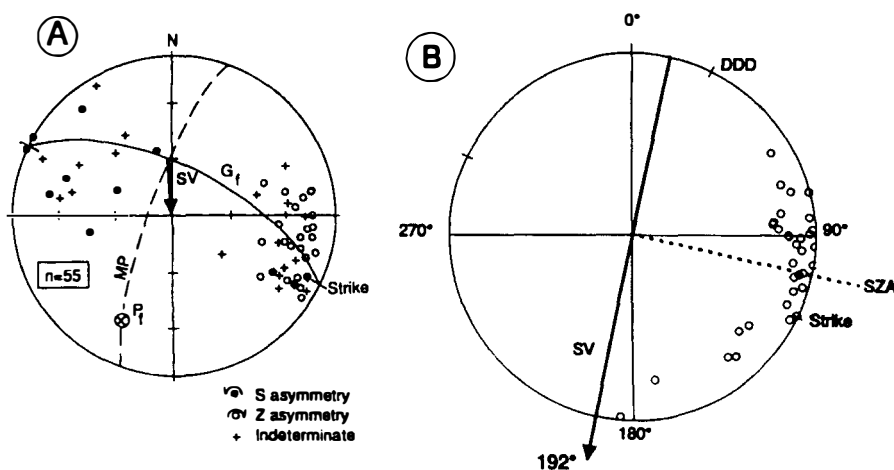


Figure 20. Synoptic analysis of mesoscale folds in the Lopez fault zone. (A) Lower-hemisphere stereogram of internal-rotation axes in present geographic orientation. G_f = average girdle for the fold axes. P_f = pole to G_f . M_p and SV are the inferred mirror plane and slip vector, respectively. (B) Fault-parallel stereogram showing Z-transformed axes. G_f was used to determine the rotation. SZA is the best-fit synoptic Z axis.

progressively obliterated toward the base of the slice; the transition to a lighter green color is due to fault-related cataclasis of the volcanic rocks. Note that mobile black mudstone flowed into the volcanic slice along narrow "veins", and that lenses of green cataclased volcanic rocks have been incorporated into the more mudstone-rich parts of the shear zone. Highly disrupted sandstone layers are present in the originally interbedded sandstone-mudstone unit below the shear zone. The penetrative cleavage in this fault zone clearly postdates the brittle deformation and cataclastic fragmentation that characterize the zone. Several generations of veins are also present: some veins are deformed by the cleavage whereas others appear to have seen little of the

cleavage-related deformation.

The small headland flanking the beach on the southeast exposes imbricated slices of green volcanic rocks and sedimentary rocks. Beds of sandstone are variably fragmented by boudinage and by slip on anastomosing faults. Some sandstone layers show lenticular shapes attributed to necking during boudinage whereas others show angular terminations. The margins of the dark green volcanic slices are locally pale green due to cataclasis. We attribute this cataclasis to the imbrication process. The elongation of sandstone

inclusions parallel to the inferred bulk shear plane for the zone is interpreted to record a general non-coaxial strain path during brittle deformation. Further shortening normal to the boundaries of this local shear zone and the Lopez Complex as a whole is recorded by the cleavage, which is subparallel to both the shear plane and the fault zone as a whole.

Kinematic indicators in the Lopez Complex are mainly restricted to asymmetric folds. Riedel structures are notably absent. Our analysis of these folds is summarized in Figures 19 and 20. The fold data are well organized and clearly indicate a top-side-to-the south sense of transport. Vergence vectors and

internal-rotation axes for the Lopez Complex show considerable variation in orientation but the degree of this variation is much less than that observed for the Rosario fault zone.

To reach Stop 2-3, take the gravel road back to Richardson and turn left (north) on Richardson Road. Go 0.8 miles and turn left (west) on Bay Road. Proceed for 1.9 miles, passing straight through the intersection with Davis Road and continuing on Burt Road. At the T-intersection, turn left (south) on Shark Reef Road and park in the small lot immediately on the right at Shark Reef Park. Follow the trail 0.3 miles west to the shoreline. We will walk south for about 0.3 miles to the edge of the park examining outcrops along

the way. The rocks are well exposed along the coastal headland. Low tide is not necessary but does allow better access to the outcrops.

Stop 2-3. Cleavage in turbidites of the Lopez Structural Complex. The purpose of this stop is to examine the SMT cleavage and to discuss the general implications of this cleavage for the kinematic evolution and exhumation of contractional wedges.

At Shark Reef Park, we can study SMT deformation of the Lopez Complex in a setting ~1.5 km below the top of the Lopez Complex. Exposed here is a coherent sequence of turbidite sandstone, mudstone, and subordinate chert-pebble conglomerate. The sequence, which is entirely upside down, dips moderately to the northeast. In comparison to Stop 2-2, these rocks show only minor brittle deformation. Of note are local arrays of sigmoidal extension gashes, small faults (slip <~5 m), and poorly defined tabular zones populated by spaced (5–10 cm) fractures. There is clear evidence of high-pressure metamorphism, as indicated by the presence of lawsonite, pumpellyite, and aragonite in the sandstones.

Subparallel to bedding is a northeast-dipping cleavage, which is penetrative in mudstones, semipenetrative in sandstones, and generally absent in the conglomerates. In outcrop, the cleavage is defined by a rough planar fissility and by flattened detrital grains. Flattened shale chips in the sandstones also provide another indication of the cleavage foliation, but these fragments may have had a preferred orientation prior to deformation. When viewed in the cleavage plane, the rock lacks any obvious linear fabric and deformed grains generally appear fairly equant. In thin sections of the sandstone, the cleavage is defined by discontinuous anastomosing selvages made up of dark insoluble minerals and by straight fiber overgrowths oriented parallel to the selvages. These straight fibers indicate that SMT deformation was approximately coaxial.

Finite strain analysis was performed on 4 sandstones from this area (7–10 in Table 1). The attitude of cleavage and the trend of **X** (equal to the orientation of the directed fiber overgrowths) are indicated in Figure 18. Note that the **X** directions are highly variable, whereas the flattening plane

show relatively little variation in attitude. Much of the distortion in these rocks was due to shortening in the **Z** direction, with strains ranging from –35 to –53 percent. Strains in the **X** and **Y** direction are fairly low, ranging from +13 to +30 percent and –10 to –22 percent, respectively. At the local scale, the strain is weakly constrictional. We note, however, that there was no extension associated with SMT strain at the regional scale (tensor average in Table 1) because local extensional strains were averaged out due to variable orientations of **X** and **Y** in the cleavage plane.

The large shortening strains in the **Z** direction were balanced by a general loss of mass from the rocks. The estimated volume strain ranges from –42 to –52 percent; we consider most, if not all, of the measured volume strain to be due to loss of mass from the rock.

Veins provide a partial record of fluid flow in these rocks. Modal measurement by linear traverses of these outcrops indicates that veins make up less than 5 percent of the rock, with the average being about 1 to 2 percent. Vein minerals include quartz and minor calcium carbonate (both calcite and aragonite). Clearly the fraction of vein material in the local outcrop does not match the fraction of mass lost from the original rock, as indicated by our strain measurements. Thus, we are forced to conclude that the dissolved mass was transported beyond the local scale of the outcrop, presumably due to pervasive and prolonged fluid flow. Furthermore, the rate and extent of SMT deformation must have been strongly controlled by the nature and extent of this fluid flow. Ongoing chemical and isotopic analyses should help to shed further light on this problem.

This stop marks the end of the field trip. To return to the Lopez Ferry Terminal, drive 1.6 miles north on Shark Reef Road until the first T-intersection. Turn right (east) on Airport Road and proceed 0.4 miles until the next T-intersection. Turn left (north) on Fisherman Bay Road and follow it 4.5 miles north passing Dill Road, Hummel Lake Road, the cutoff to Lopez Village, and Cross Road. Turn right (east) at the T-intersection with Lopez Road and then after 0.4 km turn left (north) on Ferry Road which after 3.3 miles ends at the Lopez Ferry Terminal.

References

- Babcock, R.S., and Misch, P., 1988, Evolution of the crystalline core of the North Cascades Range, in Ernst, W.G., ed., *Metamorphism and Crustal Evolution of the Western United States*, Rubey Prentice-Hall, Englewood Cliffs, N.J., v. 7, p. 214–232.
- Brandon, M.T., 1989, Geology of the San Juan–Cascade nappes, Northwestern Cascade Range and San Juan Islands, in Joseph, N.L. and others, eds., *Geologic guidebook for Washington and Adjacent Areas*: Washington Division of Geology and Earth Resources Information Circular 86, p. 137–162.
- Brandon, M.T., 1994, Representation of geologic strain data in strain–magnitude space: *Journal of Structural Geology*, in press.
- Brandon, M.T., and Cowan, D.S., 1985, The Late Cretaceous San Juan Islands–Northwestern Cascades Thrust System [abs.]: *Geological Society of America, Abstracts with Programs*, v. 17, p. 343.
- Brandon, M.T., and Cowan, D.S., 1987, The Late Cretaceous San Juan thrust system, Washington: nappes related to the arrival of Wrangellia, in Hill, M.L. ed., *Geological Society of America Centennial Field Guide—Cordilleran Section*, p. 383–388.
- Brandon, M.T., Cowan, D.S., and Vance, J.A., 1988, The Late Cretaceous San Juan Thrust System, San Juan Islands, Washington: *Geological Society of America Special Paper 221*, 81 p. and 1 plate.
- Brandon, M.T., Cowan, D.S., and Feehan, J.G., 1993, Discussion of “Kinematic analysis of the San Juan thrust system, Washington” by Maekawa, H., and Brown, E.H.: *Geological Society of America Bulletin*, v. 105, p. 839–841.
- Brown, E.H., 1987, Structural geology and accretionary history of the Northwest Cascades, Washington and British Columbia: *Geological Society of America Bulletin*, v. 99, p. 201–241.
- Brown, E.H., and Talbot, J.L., 1989, Orogen–parallel extension in the North Cascades Crystalline Core, Washington: *Tectonics*, v. 8, p. 1105–1114.
- Brown, E.H., Blackwell, D.L., Christensen, B.W., Frasse, F.I., Haugerud, R.A., Jones, J.T., Leiggi, P.L., Rady, P.M., Reller, G.J., Sevigny, J.H.,

- Silverberg, D.L., Smith, M.T., Sondergaard, J.N., and Ziegler, C.B., 1987, Geologic map of the Northwest Cascades, Washington: Geological Society of America, Map and Chart Series, MC-61, scale 1:100,000.
- Chester, F.M., and Logan, J.M., 1987, Composite planar fabric of gouge from the Punchbowl fault, California: *Journal of Structural Geology*, v. 9, p. 621-634.
- Cowan, D.S., and Brandon, M.T., 1994, A symmetry-based method for kinematic analysis of large-slip brittle fault zones: *American Journal of Science*, v. 294, p. 257-306.
- Davis, G.A., Monger, J.W.H., and Burchfiel, B.C., 1978, Mesozoic construction of the Cordilleran "collage", central British Columbia to central California, in Howell, D.G., and McDougall, K.A., eds., *Mesozoic Paleogeography of the Western United States: Society of Economic Paleontologists and Mineralogists, Pacific Section*, p. 1-32.
- England, T.D.J., and Calon, T.J., 1991, The Cowichan fold and thrust system, Vancouver Island, southwestern British Columbia: *Geological Society of America Bulletin*, v. 103, p. 336-362.
- Hansen, E., 1971, *Strain Facies*: New York, Springer-Verlag, 207 p.
- Haugerud, R.A., Van Der Heyden, P., Tabor, R.W., Stacey, R.W., and Zartman, R.E., 1991, Late Cretaceous and early Tertiary plutonism and deformation in the Skagit Gneiss Complex, North Cascade Range, Washington and British Columbia: *Geological Society of America Bulletin*, v. 103, p. 1297-1307.
- Johnson, S.Y., Zimmerman, R.A., and Naeser, C.W., 1986, Fission-track dating of the tectonic development of the San Juan Islands, Washington: *Canadian Journal of Earth Sciences*, v. 23, p. 1318-1330.
- Journeay, J.M., and Friedman, R.M., 1993, The Coast Belt Thrust System: Evidence of Late Cretaceous shortening in southwest British Columbia: *Tectonics*, v. 12, p. 756-775.
- Kamb, W.B., 1959, Ice petrofabric observations from Blue Glacier, Washington, in relation to theory and experiment: *Journal of Geophysical Research*, v. 64, p. 1891-1909.
- Logan, J.M., Friedman, M., Higgs, N., Dengo, C., and Shimamoto, T., 1979, Experimental studies of simulated gouge and their application to studies of natural fault zones, in *Proceedings of Conference VIII on Analysis of Actual Fault Zones in Bedrock*: U.S. Geological Survey Open-File Report 79-1239, p. 305-343.
- Maekawa, H. and Brown, E.H., 1991, Kinematic analysis of the San Juan thrust system, Washington: *Geological Society of America Bulletin*, v. 103, p. 1007-1016.
- Maekawa, H. and Brown, E.H., 1993, Reply to discussion of "Kinematic analysis of the San Juan thrust system, Washington": *Geological Society of America Bulletin*, v. 105, p. 841-844.
- McGroder, M.F., 1989, Structural geometry and kinematic evolution of the eastern Cascades foldbelt, Washington and British Columbia: *Canadian Journal of Earth Sciences*, v. 26, p. 1586-1602.
- McGroder, M.F., 1991, Reconciliation of two-sided thrusting, burial metamorphism, and diachronous uplift in the Cascades of Washington and British Columbia: *Geological Society of America Bulletin*, v. 103, p. 189-209.
- Means, W.D., Hobbs, B.E., Lister, G.S., and Williams, P.F., 1980, Vorticity and non-coaxiality in progressive deformation: *Journal of Structural Geology*, v. 2, p. 371-378.
- Miller, R.B., Brown, E.H., McShane, D.P., and Whitney, D.L., 1993, Intra-arc crustal loading and its tectonic implications, North Cascades crystalline core, Washington and British Columbia: *Geology*, v. 21, p. 255-258.
- Misch, P., 1966, Tectonic evolution of the northern Cascades of Washington State—a west-Cordilleran case history: *Canadian Institute of Mining and Metallurgy, Special Volume 8*, p. 101-148.
- Monger, J.W.H., Price, R.A., and Tempelman-Kluit, D.J., 1982, Tectonic accretion and the origin of two major metamorphic and plutonic belts in the Canadian Cordillera: *Geology*, v. 10, p. 70-75.
- Palumbo, G.T.X., and Brandon, M.T., 1990, Gravity modeling of the geometry of the frontal thrust to the Late Cretaceous San Juan nappes, NW Washington State [abs.]: *Geological Society of America, Abstracts with Program*, v. 22, no. 7, p. A325.
- Paterson, M.S., and Weiss, L.E., 1961, Symmetry concepts in the structural analysis of deformed rocks: *Geological Society of America Bulletin*, v. 72, p. 841-882.
- Platt, J.P., 1986, Dynamics of orogenic wedges and the uplift of high-pressure metamorphic rocks: *Geological Society of America Bulletin*, v. 97, p. 1037-1053.
- Ramsay, J.G., and Huber, M.I., 1983, *The Techniques of Modern Structural Geology, Volume 1: Strain Analysis*: London, Academic Press., 307 p.
- Ring, U., and Brandon, M.T., 1994, Kinematic analysis of heterogeneous brittle deformation on the Coast Range fault zone: Implications for contractional deformation and exhumation of the Franciscan subduction complex (California Coast Ranges): *Geological Society of America Bulletin*, in review.
- Rubin, C.M., Saleeby, J., Cowan, D.S., Brandon, M.T., and McGroder, M.F., 1990, Regionally extensive mid-Cretaceous west-vergent thrust system in the northwestern Cordillera: Implications for continent-margin tectonism. *Geology*, v. 18, p. 276-280.
- Rutter, E.H., Maddock, R.H., Hall, S.H., and White, S.H., 1986, Comparative microstructures of natural and experimentally produced clay-bearing fault gouges: *Pure and Applied Geophysics*, v. 124, p. 3-30.
- Selverstone, J., 1985, Petrologic constraints on imbrication, metamorphism, and uplift in the SW Tauern window, Eastern Alps: *Tectonics*, v. 4, p. 687-704.
- Smith, M., 1988, Deformational geometry and tectonic significance of a portion of the Chilliwack Group, northwestern Cascades, Washington: *Canadian Journal of Earth Sciences*, v. 25, p. 433-441.
- Twiss, R.J., and Gefell, N.J., 1990, Curved slickenfibers: a new brittle shear sense indicator with application to a sheared serpentinite: *Journal of Structural Geology*, v. 12, p. 471-481.
- Wallis, S.R., Platt, J.P., and Knott, S.D., 1993, Recognition of syn-convergence extension in accretionary wedges with examples from the Calabrian arc and the eastern Alps: *American Journal of Science*, v. 293, p. 436-496.